Bioconjugate Chemistry

Article

pubs.acs.org/bc

Peptidyl–Oligonucleotide Conjugates Demonstrate Efficient Cleavage of RNA in a Sequence-Specific Manner

Aled Williams,*[,†,#] Yaroslav Staroseletz,[‡,#] Marina A. Zenkova,[‡] Laurent Jeannin,[§] Harmesh Aojula,[†] and Elena V. Bichenkova[†]

[†]Manchester Pharmacy School, University of Manchester, Oxford Road, Manchester, United Kingdom, M13 9PT

[‡]Institute of Chemical Biology and Fundamental Medicine SB RAS, 8 Laurentiev Avenue, 630090, Novosibirsk, Russia

[§]Peptisyntha S.A., 310 Rue de Ransbeek, 1120 Brussels, Belgium

Supporting Information

ABSTRACT: Described here is a new class of peptidyl–oligonucleotide conjugates (POCs) which show efficient cleavage of a target RNA in a sequence-specific manner. Through phosphoramidate attachment of a 17-mer TΨC-targeting oligonucleotide to amphiphilic peptide sequences containing leucine, arginine, and glycine, zero-linker conjugates are created which exhibit targeted phosphodiester cleavage under physiological conditions. $tRNA^{Phe}$ from brewer's yeast was used as a model target sequence in order to probe different structural variants of POCs in terms of selective TΨC-arm directed cleavage. Almost quantitative (97–100%) sequence-specific tRNA cleavage is observed for several POCs over a 24 h period with a reaction half-life of less than 1 h. Nontargeted cleavage of $tRNA^{Phe}$ or HIV-1 RNA is absent. Structure–activity relationships reveal that removal of the peptide's central glycine residue significantly decreases tRNA cleavage activity; however, this can be entirely restored through replacement of the peptide's C-terminal carboxylic acid group with the carboxamide functionality. Truncation of the catalytic peptide also has a detrimental effect on POC activity. Based on the encouraging results presented, POCs could be further developed with the aim of creating useful tools for molecular biology or novel therapeutics targeting specific messenger, miRNA, and genomic viral RNA sequences.

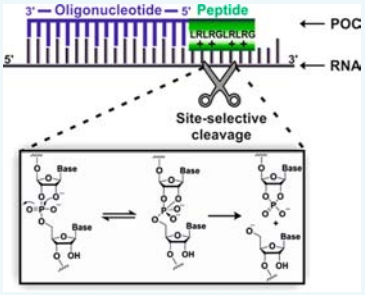

INTRODUCTION

Sequence-specific RNA cleavage is an attractive prospect that could have uses in the fields of biotechnology, molecular biology, and RNA-silencing therapeutics.[1,2] For example, selective targeting and cleavage of specific mRNA sequences encoding disease-relevant proteins[3] or micro-RNAs[4] associated with diverse types of cancer may potentially expand the therapeutic window for drug discovery and allow new selective therapies to be developed.

A variety of RNA-silencing methods are currently used which are covered in detail elsewhere[4,5] and will not be discussed here. Recently, however, it has been shown that cellular delivered small-interfering RNAs (siRNAs) can have a negative impact on "normal" cellular biochemistry by saturating the RNA-induced silencing complex (RISC).[6] As a consequence, certain genes and their corresponding proteins (including oncogenes: HMGA2, CCND1, and DUSP2) can be up-regulated to nonphysiological levels, an effect which may perturb the down-regulation of the desired gene.[6]

RNA-mediated controlled translational arrest can also be achieved by using reactive oligonucleotide analogues which may be directed and controlled chemically toward particular RNA sequences, leading to efficient gene expression knockdown, without any complex cellular cascades triggered by siRNA gene silencing.[7−9] Through attachment of an RNA cleaving molecule (discussed later) to an antisense oligonucleotide (ASO), it is possible to cleave structured RNA molecules without the requirement of any additional enzymes or cofactors, such as those associated with RISC.[7−9] The cleaving moiety acts to mimic the active site of a ribonuclease, while the ASO delivers it to the desired RNA region, thus increasing its effective concentration. At physiological pH the cleavage reaction occurs via a transesterification of the 2′-oxyanion onto the adjacent phosphorus atom leading to a dianionic phosphorane intermediate.[10,11] This proceeds to breakdown via departure of the 5′-linked nucleoside, forming a 2′,3′-cyclic phosphate (Figure 1). The presence of the 2′ hydroxyl group makes RNA susceptible to cleavage ($\tau^{1/2}$ = 100 years, pH 7, 23 °C); however, it is possible to catalyze the cleavage reaction by (i) enhancing the rate of deprotonation at 2′ hydroxyl group (rate enhancement (RE) ≈ 10^6); stabilizing (ii) the phosphorane intermediate (RE ≈ 10^5) or (iii) the leaving group (RE ≈ 10^6); (iv) promoting the required "in-line" geometry when the 2′ oxyanion enters (or the 5′ linked nucleotide leaves) the phosphorane intermediate (RE ≈ 100-fold).[12] Numerous artificial (or chemical) ribonucleases have been developed that are able to catalyze this single-stranded RNA cleavage with the cleaving group taking one of many forms. Some examples

Received: April 10, 2015
Revised: May 6, 2015
Published: May 8, 2015

DOI: 10.1021/acs.bioconjchem.5b00193
Bioconjugate Chem. 2015, 26, 1129−1143

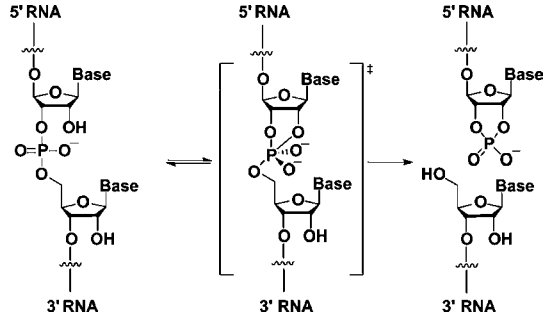

Figure 1. RNA cleavage via phosphodiester transesterification.

include metal complexes (copper,[13−15] dysprosium,[16] europium,[17] zinc[18,19]); imidazole scaffolds;[20] base-pair mimics;[21] acridine derivatives;[22] mono- and diazacrowns;[23−25] oligopeptides.[8,9] Although some metal-dependent artificial ribonucleases display high ribonuclease activity in vitro,[16,26−28] they suffer from a number of disadvantages, e.g., uncontrolled diffusion of radicals, which creates a risk for degradation of nontarget biopolymers. Therefore, the development of metal-independent RNA-cleaving conjugates capable of cleaving RNA efficiently without additional exogenous cofactors (i.e., metal ions, oxygen, redox reagents) would be advantageous as they eliminate the risk of metal loss from the coordinating ligand. In recent years a number of such metal-independent sequence-specific chemical ribonucleases have been designed and synthesized.[7−9] However, their hydrolytic activity against RNA remains to be inferior to that of the metal ion dependent artificial ribonuclease, as well as their natural counterparts. Recently discovered peptidyl-oligonucleotide constructs[8,9] generated by chemical fusion of a short, synthetic peptide containing a regular stretch of alternating basic (e.g., arginine, lysine) and hydrophobic (e.g., leucine, alanine) residues with short noncomplementary oligonucleotides have shown enhanced hydrolytic activity and multiple catalytic turnover against various RNA sequences (e.g., short synthetic RNA, in vitro transcripts of 96-nt fragment of RNA HIV-1 and human $tRNA_3^{Lys}$). The most remarkable feature of these chemical nucleases was that the short DNA fragment was able to considerably enhance the biological activity of the otherwise inactive peptide. Although these chemical ribonucleases showed distinctive cleavage patterns (e.g., G-X, Pyr-A, G-X > Pyr-A or G-X < Pyr-A), they can only be classed as base-specific as they recognize only a single residue (e.g., G) or particular dinucleotide blocks (e.g., C-A or U-A) as a target point for RNA cleavage. Since any mono- and dinucleotide blocks are highly abundant in every RNA molecule, these chemical ribonucleases suffer from a lack of sequence-specificity, as they are not capable of identifying a unique stretch of RNA, which may lead to irreversible damage of "normal" physiological function. From a therapeutic standpoint this would lead to high cytotoxicity, thus questioning their potential application for gene silencing. Our main challenge therefore was to achieve a high level of sequence-specificity, to enable cleavage of the RNA target at a predetermined location, while retaining (or improving) catalytic efficiency of such peptidyl−oligonucleotide conjugates. This work presents a new class of sequence-specific, catalytic POCs containing a variety of amphiphilic peptides covalently attached to an antisense 17-mer oligonucleotide (pGATCGAACACAGGACCT; Oligonucleotide **A**), targeting the TΨC region of brewer's yeast $tRNA^{Phe}$. Although a clinically irrelevant target, the common structural elements present in $tRNA^{Phe}$ make it a suitable starting point to develop and optimize POCs for a new generation of RNA targeting therapeutics. In addition, thorough investigations into the hybridization properties of antisense oligonucleotides with this target have already been carried out.[29,30] We report here a comprehensive analysis of the catalytic activity, sequence-selectivity, and structure−activity relationships of these new POC analogues against $tRNA^{Phe}$ as a model RNA target and demonstrate the effect of various structural alterations on their performance.

RESULTS AND DISCUSSION

Peptide and Peptidyl−Oligonucleotide Conjugate Synthesis and Characterization. The core peptide sequences chosen for synthesis (see Figure 2) were based upon the polycationic peptide $[LR]_4G\text{-}CONH_2$ containing leucine-arginine building blocks, which showed RNase T1 and/or RNase A like cleavage activity when conjugated to a short oligonucleotide (e.g.$(pdRib)_3$GGATCTCTT, pGGAT, pTCTCTC).[8,9] Arginine-rich elements are common in RNA-binding proteins as they are able to interact strongly with guanine residues via hydrogen bonding and phosphate groups through electrostatic interactions.[31−36] To investigate the influence of the peptide length on the catalytic activity of the peptidyl−oligonucleotide conjugates, we synthesized two oligopeptides with differing numbers of the repeating [LR] unit (LRLRG and LRLRLRLRG, P2 and P4, respectively). Additionally, a peptide containing this repeating motif, but with the addition of a central glycine residue at position 5, was synthesized (LRLRGLRLRG; P4G) in order to enhance conformational flexibility of the cleaving construct. Glycine residues play a crucial role in the active sites of many enzymes as they provide a degree of conformational freedom to accommodate substrate binding and catalysis.[37−40] Yan et al.[37] also report that many enzyme active sites are rich in G-X-Y or Y-X-G motifs, where X and Y are polar and nonpolar residues, respectively, akin to leucine and arginine used here. Finally, two C-terminal variants of P4 and P4G core peptides were synthesized (carboxylic acid and carboxamide, e.g., P4-COOH and $P4\text{-}CONH_2$) in order to investigate whether the peptide C-terminal chemistry could alter the RNA binding and cleavage properties. The structures and nomenclature of five different peptides used in this research as catalytic elements within the POCs are shown in Figure 2.

Peptides were synthesized using an Fmoc-Gly-Wang resin (C-terminal carboxylic acid) (215 mg, 0.2 mmol) or an Fmoc-Gly-Rink Amide-MBHA resin (C-terminal carboxamide) (430 mg, 0.18 mmol) and manual solid-phase methodology utilizing the common Fmoc/^{t}Bu protocol. The 2,2,4,6,7-pentamethyldihydrobenzofuran-5-sulfonyl (Pbf) group was chosen as the protecting group for arginine. This can be removed by TFA in conjunction with resin cleavage. The peptides were purified by semipreparative RP-HPLC and characterized using 1D and 2D NMR techniques as well as electrospray ionization mass spectrometry (ESI-MS). The detailed information on synthesis, purification and characterization is given in the Experimental Procedures section.

Five different POCs incorporating the same 17-mer oligonucleotide pGATCGAACACAGGACCT (oligonucleotide **A**), but different catalytic peptides (Figure 2) were synthesized according to Zarytova et al.[41] This method uses the DMSO-soluble, cetyltrimethylammonium bromide salt of oligonucleotide **A**, along with activating agents triphenylphosphine, 2,2′-

DOI: 10.1021/acs.bioconjchem.5b00193
Bioconjugate Chem. 2015, 26, 1129−1143

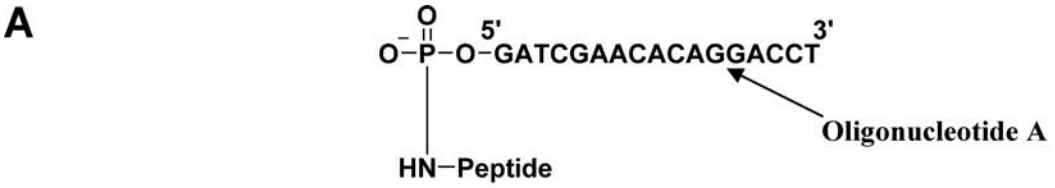

B

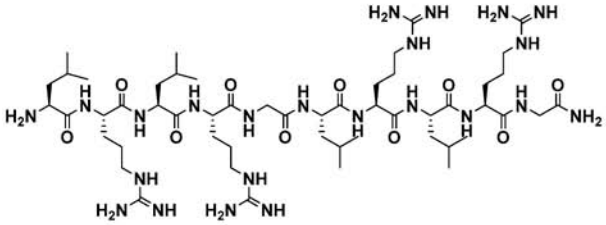

P4G-CONH$_2$ (1)

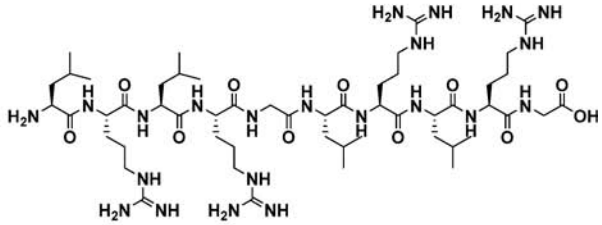

P4G-COOH (2)

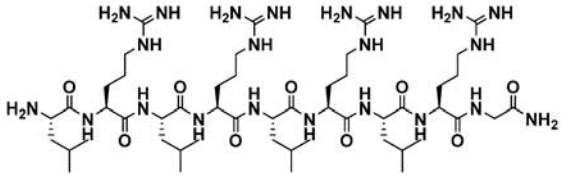

P4-CONH$_2$ (3)

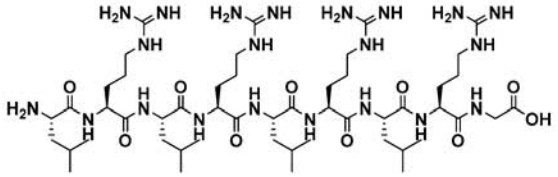

P4-COOH (4)

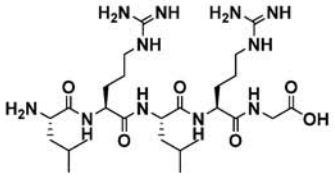

P2-COOH (5)

C

P4G-A-COOH	(6)
P4G-A-CONH$_2$	(7)
P4-A-COOH	(8)
P4-A-CONH$_2$	(9)
P2-A-COOH	(10)

Figure 2. A. Schematic representation of a general structure of POCs containing the same 17-mer oligonucleotide A, but different peptide fragments. B. Peptide structures and nomenclature. C. POC nomenclature.

dipyridyl disulfide, and 4-(dimethylamino)pyridine. The amide-protected C-terminal of the carboxamide peptides allowed these to be used directly in the reaction conditions. The C-terminal carboxylic acid peptides, however, required the oligonucleotide to be preactivated before the peptide was added. This prevented peptide self-condensation from occurring. Providing all solvents are anhydrous, the oligonucleotide is stable in this DMAP-preactivated state. The peptides were used as lyophilized TFA-salts with no further modifications required. Various reaction conditions (e.g., reagent excess, volume, temperature, time) were sequentially modified to find the optimum for conjugate yield, with the biggest contributory factors being minimal reaction volume and reagent excess (data not shown). Conjugate products were isolated by precipitation with 4% $LiClO_4$ (w/v) in acetone and purified by RP-HPLC. A retention time shift of between 2 to 6 min is observed due to

DOI: 10.1021/acs.bioconjchem.5b00193
Bioconjugate Chem. 2015, 26, 1129−1143

the conjugation (dependent on the length of the peptide) compared to unmodified oligonucleotide **A**. Reproducible yields between 70% and 90% were achievable. As expected, the conjugates containing the C-terminal carboxamide group had a longer retention time than their corresponding C-terminal acid form. In the following sections, peptides and POCs will be referred to as outlined in Figure 2. Identity and purity of the synthesized POCs have been confirmed by RP-HPLC, Urea-PAGE, ^{1}H and ^{31}P NMR spectroscopy, and mass spectrometry (see Experimental Procedures and Supporting Information).

Although full assignment of ^{1}H NMR signals of POCs is convoluted by the numerous overlapping signals in the peptide regions and oligonucleotide sugar ring areas of the spectra (0.5−4.7 ppm), it was possible to confidently confirm successful conjugation via comparison of ^{1}H NMR spectra of conjugates with those of the starting materials (i.e., unmodified oligonucleotide and free peptides). As an example, Figure 3A shows ^{1}H NMR spectrum of P4G-A-COOH (bottom) in comparison with that for unmodified oligonucleotide **A** (top). The appearance of new distinctive signals in the area of 0.5−0.8 ppm and 2.8−3.2 ppm characteristic to the Leu-H$^{\delta}$, and Arg-H$^{\beta}$, respectively, in addition to the oligonucleotide signals, which are seen in both spectra, signifies the presence of both components in the reaction products. Although the other peptide protons (i.e., Arg-H$^{\gamma,\delta}$ and Leu-H$^{\beta,\gamma}$ at 1.0−2.7 ppm, as well as Arg-H$^{\alpha}$, Leu-H$^{\alpha}$, and Gly-H$^{\alpha}$ at 3.5−4.5 ppm) strongly overlap with the methyl and sugar ring protons of the oligonucleotide component, they provide additional evidence of successful incorporation of the peptide component into the conjugate structure. Careful integration of the ^{1}H NMR signals in the oligonucleotide aromatic (7.2−8.4 ppm) and H1′/Ar−H5 (5.4−6.4 ppm) regions as well as those generated by Leu-H$^{\delta}$ and Arg-H$^{\beta}$ protons (0.5−0.8 ppm and 2.8−3.2 ppm, respectively) allowed evaluation of precise stoichiometric ratio between oligonucleotide and peptide components. Indeed, by using a single nucleotide aromatic signal for internal integral calibration, it was possible to confirm that there was a 1:1 ratio of oligonucleotide to peptide present. In addition, ^{31}P NMR analyses (Figure 3 B) of all of the POCs show the characteristic shift (∼7 ppm) of the 5′-terminal ^{31}P signal (bottom) upon peptide conjugation as compared with that seen for the unconjugated oligonucleotide **A** (top).

Finally, matrix-assisted laser desorption spectroscopy (MALDI) gave molecular ion peaks which corresponded well with the theoretical molecular masses (see Experimental Procedures and Supporting Information). The homogeneity of oligonucleotide **A** and POCs were also tested by Urea-PAGE and were shown to be between 95% and 100% (see Supporting Information). Urea-PAGE analysis also demonstrates the reduced electrophoretic mobility of the POCs compared to unconjugated oligonucleotide **A**.

Hybridization of POCs to tRNA^{Phe}. tRNA^{Phe} was chosen deliberately as the target to assess the cleavage activity because many other types of oligonucleotide-based artificial ribonucleases have been tested using this target.[20,42−45] Moreover, hybridization of antisense oligonucleotides with yeast tRNA^{Phe} has been investigated in detail providing useful background for comparison.[29,30,46] In addition, the short sequence (relative to other natural RNAs) allows us to detect cleavage patterns directly using end-labeled RNA species.

Figure 4 represents the cloverleaf structure of yeast tRNA^{Phe} showing the target site for the designed POCs containing the 17-mer oligonucleotide **A** complementary to the tRNA^{Phe} sequence 44−60. Hybridization of **A** with the 44−60 sequence results in delivery of the conjugated catalytic peptide to the two

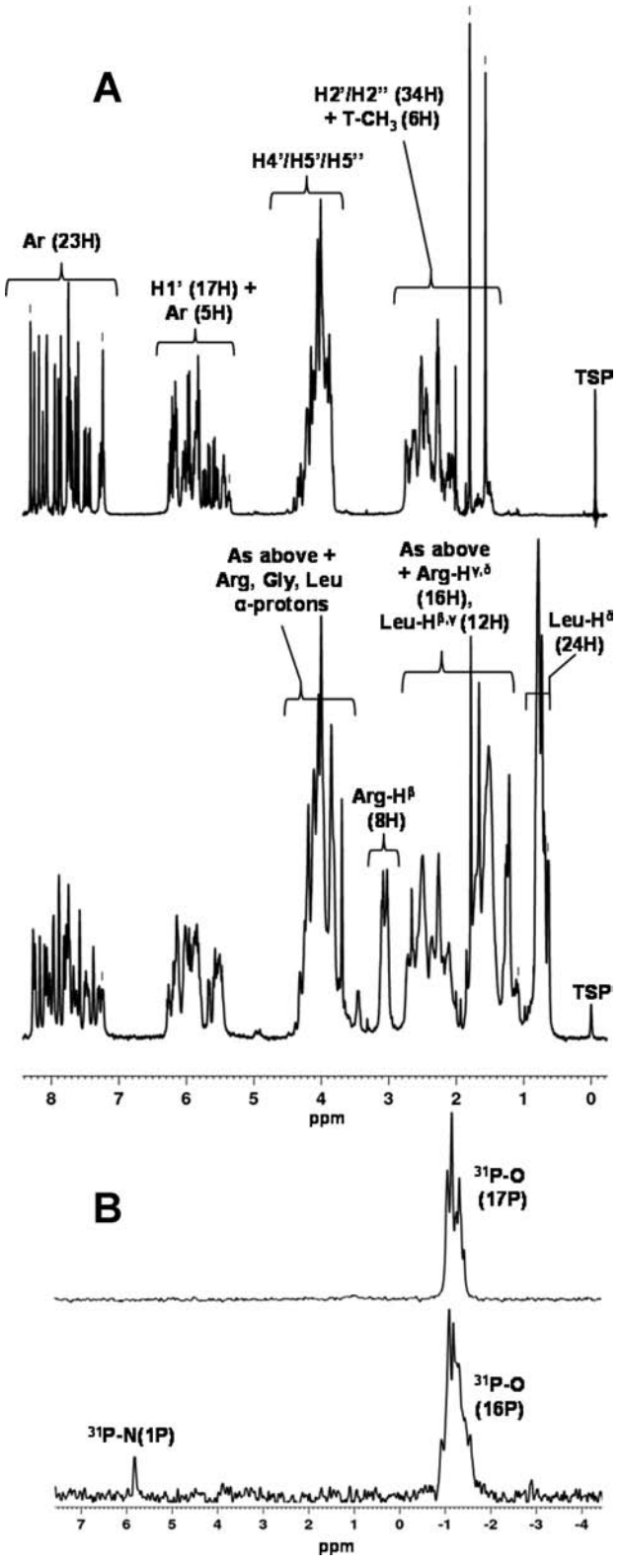

Figure 3. A. ^{1}H NMR spectra of Oligonucleotide **A** (top) and P4G-A-COOH (bottom), showing the addition of characteristic peptide resonances. B. ^{31}P NMR spectra of Oligonucleotide **A** (top) and P4G-A-COOH (bottom) showing the characteristic downfield shift of the 5′-terminal ^{31}P signal upon conjugation to P4G.

DOI: 10.1021/acs.bioconjchem.5b00193
Bioconjugate Chem. 2015, 26, 1129−1143

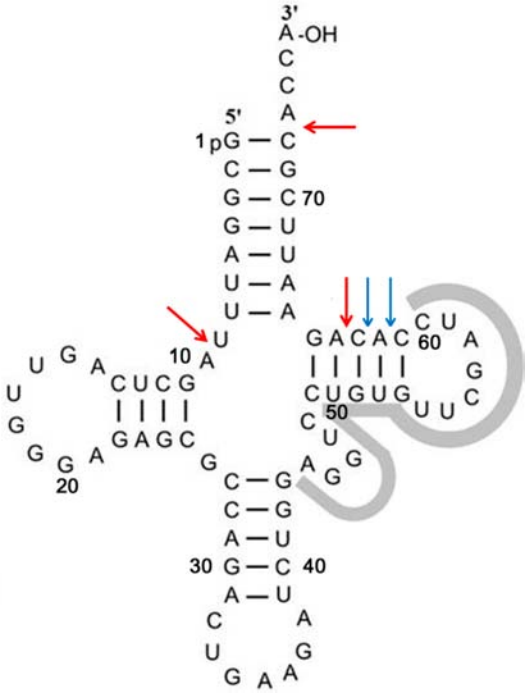

Figure 4. Secondary structure of in vitro transcript of $tRNA^{Phe}$. Red and blue arrows show major and minor RNA cleavage sites with peptidyl−oligonucleotide conjugates, respectively. Oligonucleotide **A** (GATCGAACACAGGACCT) complementary to the tRNA residues 44−60 is shown as a gray line.

adjacent CA bonds in the sequence ^{61}CACAG^{65} that are particularly susceptible to cleavage by small ribonuclease mimics.[47] Upon binding with POCs, the TΨC arm unfolds, forcing the target region to become single-stranded and thus a suitable site for cleavage.

The ability of the POCs to hybridize with their target tRNA sequence was determined by a gel-retardation method (Figure 5). This was carried out by incubating 3′-fluorescein isothiocyanate (FITC) labeled $tRNA^{Phe}$ (here and after FITC-$tRNA^{Phe}$) in a standard buffer with increasing concentrations of the POCs (see Experimental Procedures) followed by analysis of the reaction mixtures on 10% native PAGE. The time scale of the experiment ensures any $tRNA^{Phe}$ cleavage is minimized. Binding of the $tRNA^{Phe}$ to the POC resulted in a heteroduplex formation with a different electrophoretic mobility as compared to the unbound $tRNA^{Phe}$. It has been shown previously using this technique that oligonucleotide **A** is able to bind efficiently to its target sequence within $tRNA^{Phe}$ ($K_a = (7.0 \pm 1) \times 10^6\ M^{-1}$).[20] Notably, hybridization with this oligonucleotide resulting in the unfolding of the TΨC hairpin does not disturb the other secondary structural elements of the rest of the tRNA molecule.[48]

It is seen from Figure 5C that the association constants obtained for POCs are lower in comparison with that of parent oligonucleotide **A** by a factor of 7 and 14 for P4G-A-COOH and P4-A-COOH, respectively. Although peptide P4G-COOH is longer than peptide P4-COOH, the added flexibility of an additional glycine residue may allow for a more energetically favorable interaction of P4G-A-COOH with tRNA. P2-A-COOH containing the shortest peptide perturbs tRNA binding the least. Saturation binding is nevertheless achieved for all

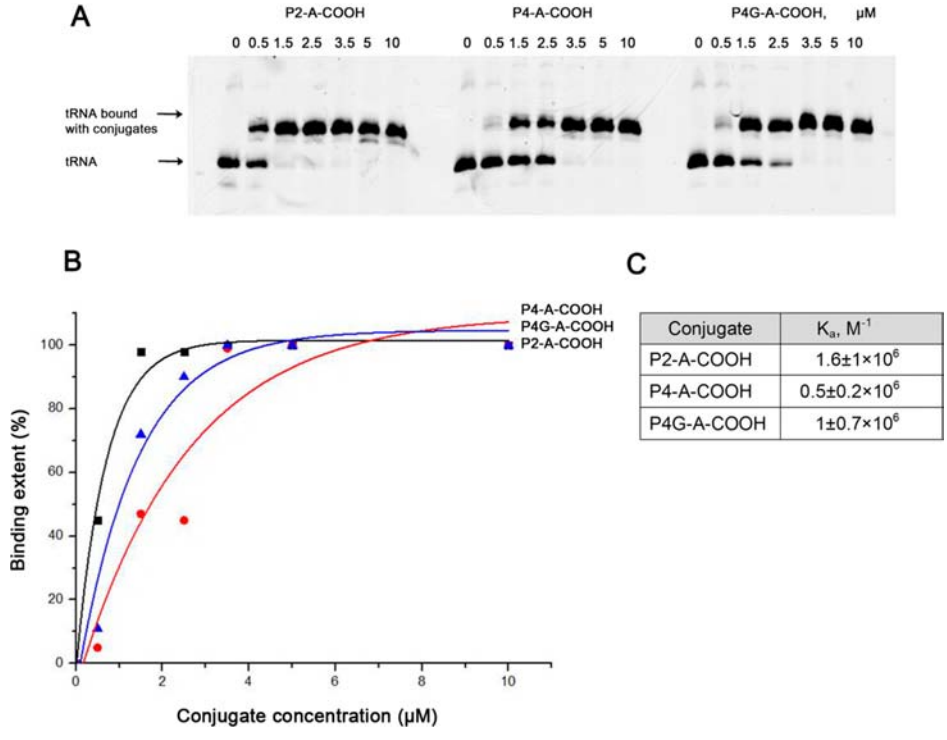

Figure 5. Gel-shift analysis of hybridization of the P2-A-COOH, P4-A-COOH, and P4G-A-COOH conjugates with 3′-FITC-$tRNA^{Phe}$ (0.5 μM). A. Representative images of the PAGE showing binding of the P2-A-COOH, P4-A-COOH, and P4G-A-COOH conjugates with fluorescently labeled $tRNA^{Phe}$. The conjugate type and concentrations are shown at the top. Arrows show unbound tRNA and tRNA−conjugate complex. B. Secondary plot of the data, shown in A. C. Association constants of 3′-FITC- $tRNA^{Phe}$ binding with the conjugates evaluated using the equation $K_a = \alpha/[\text{Conj}](1 - \alpha)$ where α is binding extent, [Conj] is concentration of the conjugate.

DOI: 10.1021/acs.bioconjchem.5b00193
Bioconjugate Chem. 2015, 26, 1129−1143

three POCs between POC:tRNA^{Phe} ratios of 3:1 and 7:1. Association constants were found to be in the μM range for P2-A-COOH, P4-A-COOH, and P4G-A-COOH. Binding efficiencies of carboxamide-containing conjugates P4-A-CONH$_2$ and P4G-A-CONH$_2$ were similar to those of their structural analogues P4-A-COOH and P4G-A-COOH (data not shown), showing that the COOH group does not perturb binding, which could be expected due to charge repulsion. In addition, the presence of a single band shift is indicative of 1:1 tRNA:POC binding stoichiometry, implying that imperfect tRNA:POC complexes are nonfavorable.

Cleavage of Yeast tRNA^{Phe} by P4G-A-COOH Conjugate. The cleavage activities of the conjugates were assayed under physiological conditions (37 °C, pH 7.4, Tris-buffered) against FITC-tRNA^{Phe} (1 μM, see Experimental Procedures for conditions). Tris-buffer is commonly used in RNA cleavage experiments because it does not interfere with the RNA transesterification process.[17,49,50] Additionally, incorporation of 1 mM EDTA removed the possibility of undesirable metal-ion induced RNA cleavage. Cleavage products were analyzed by electrophoresis in 12% PAGE under denaturing conditions. RNase T1 and imidazole tRNA^{Phe} hydrolysis ladders were used to identify cleavage sites. Figure 6A shows the typical pattern of tRNA^{Phe} cleavage with P4G-A-COOH under physiological conditions. No spontaneous cleavage of tRNA is seen under these conditions in the absence of the POC (see lane C, in Figure 6A). Similarly, no tRNA cleavage is observed when incubated with either the parent oligonucleotide A or nonattached peptide (data not shown). This data is consistent with our previous results showing that peptide $[LR]_4G$ displays RNA cleavage activity only when conjugated with oligonucleotide.[9]

The conjugates cleave RNA primarily at the target site with the major cut at C63-A64 and additional minor cleavages at sites C61-A62 and A62-C63. The ratios between tRNA cleavage products at C63-A64 and C61-A62/A62-C63 sequences adjacent to each other are presumably consistent with the steric availability of these sites toward cleavage by POCs.[45] Besides these sites, two additional phosphodiester bonds (i.e., U8-A9 and C72-A73) outside the target sequence were cleaved with efficiency close to that of the C63-A64 site (Figure 4 and Figures 6A, 7A, and 8). The regions U8-A9 and C73-A74 are highly sensitive to the cleavage by ribonucleases and by RNase mimics.[44,51−53] The cleavage of these two additional sites may result from sequence-specific cleavage presumably due to the close proximity of the U8-A9 linkage to the target sequence within the tRNA^{Phe} tertiary structure and due to the sufficient length of the peptide within the POC (discussed later). We can exclude the possibility of spontaneous tRNA cleavage within the heteroduplex. Additionally, it is worth noting that the cleavage products migrated similarly to oligonucleotides generated by RNase T1 or by 2 M imidazole treatment (Figure 6A, Lanes Im and T1, respectively), indicating formation of a cyclic phosphodiester at the 3′-cleavage site, and a hydroxyl group in the 5′-cleavage products.

Figure 6B shows the concentration dependency of the cleavage reaction for P4G-A-COOH. It can be seen that a plateau cleavage activity is reached at a POC concentration of between 10 and 20 μM. At this concentration, we would expect the POC to be under conditions of complete binding. Therefore, no further increases in conjugate concentration will alter the cleavage activity. Interestingly, after the plateau is reached (Figure 6A, lanes 20 and 40) the relative intensities of

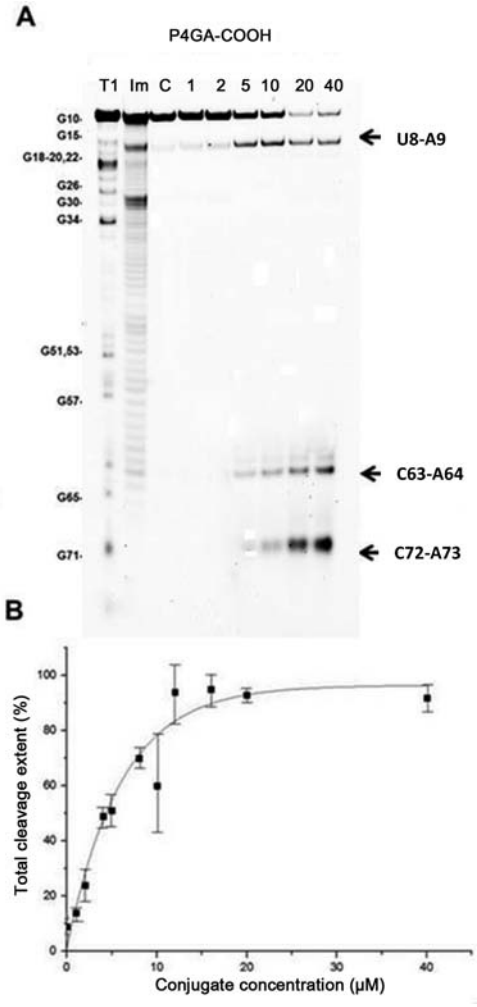

Figure 6. Concentration dependence of 3′-FITC-tRNA^{Phe} cleavage with P4G-A-COOH. A. Image of 12% PAA/8 M urea gel after electrophoresis of 3′-FITC-tRNA^{Phe} cleavage products. 3′-FITC-tRNA^{Phe} (1 μM) was incubated with various concentrations of P4G-A-COOH (indicated in the top) at 37 °C for 24 h. Lanes T1 and Im, partial RNA digestion with RNase T1 and 2 M imidazole buffer, respectively. Positions of RNA cleavage with the conjugate and RNase T1 are shown on the right and left, respectively. B. Dependence of RNA cleavage extent on conjugate concentration. Data of three independent experiments. The standard deviations were calculated using *Origin 8*.

the bands U8-A9 and C72-A73 change. This can be explained by the putative mechanism of RNA cleavage implying that cleavage at three major sites seems to occur simultaneously with the formation of different tRNA fragments; these undergo further cleavage within the heteroduplex, resulting in the shortest label-bearing RNA fragment being formed (C72-A73). Notably, no other regions except for those mentioned above are cleaved by POCs within tRNA^{Phe}.

The noticeable difference observed between the extent of binding (Figure 5B) and the extent of tRNA cleavage (Figure 6B) is to be expected, as the target concentration used for the cleavage assay (1 μM) is twice that of the target concentration used in the gel-shift assay (0.5 μM) (Note: this is to improve signal-to-noise of fluorescently labeled RNA fragments). Based on the data presented in Figure 5, at a P4G-A-COOH concentration of 7 μM we would expect maximum binding to occur. However, the observed cleavage extent of tRNA^{Phe} at this

DOI: 10.1021/acs.bioconjchem.5b00193
Bioconjugate Chem. 2015, 26, 1129−1143

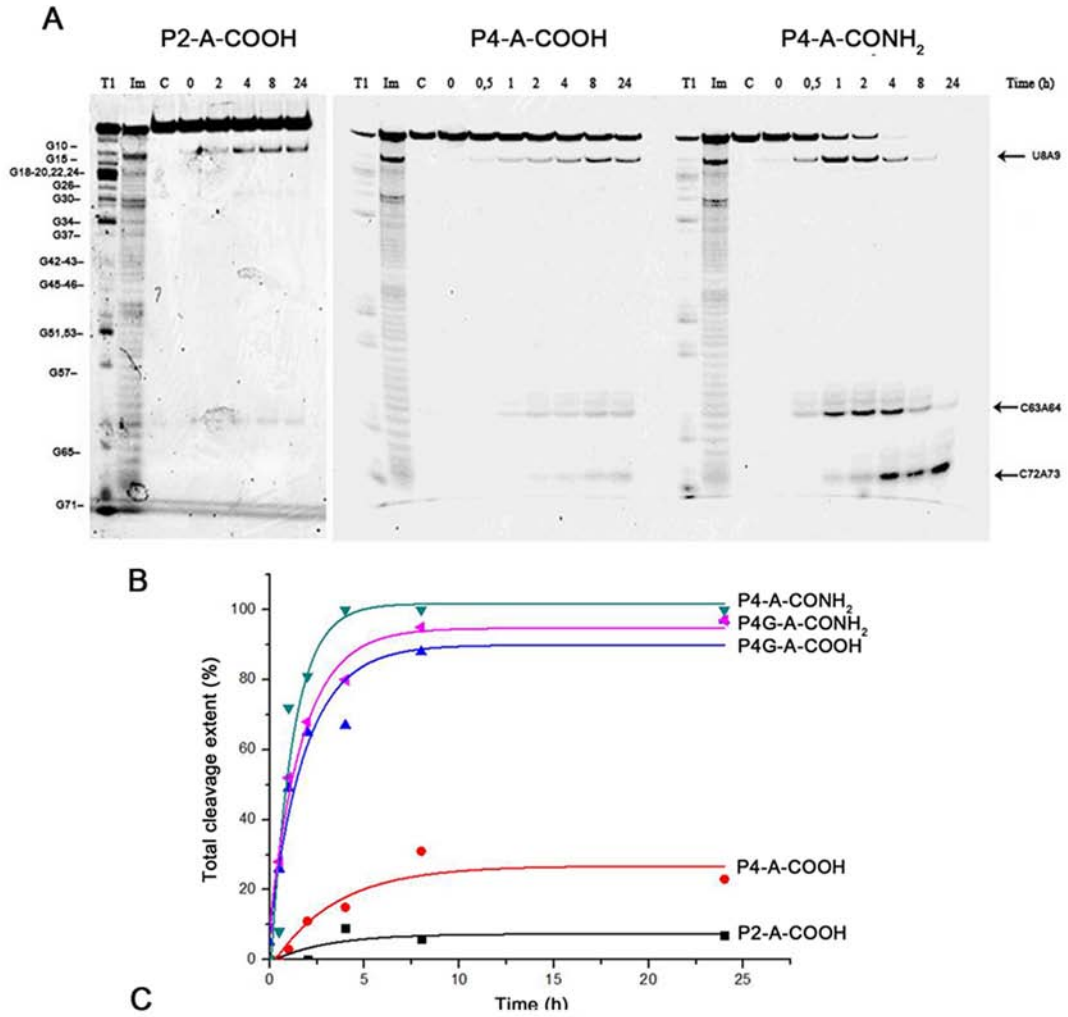

C

Name	Structure(3'→5'), N→C)	Binding extent, %	Cleavage extent (24h, 20μM), %
P2-A-COOH	$^{3'}$OligonucleotideA$^{5'}$-LRLRG-COOH	100	7±2
P4-A-COOH	$^{3'}$OligonucleotideA$^{5'}$-LR(LR)$_3$G-COOH	100	24±3
P4G-A-COOH	$^{3'}$OligonucleotideA$^{5'}$-LRLRG(LR)$_2$G-COOH	100	97±8
P4-A-CONH$_2$	$^{3'}$OligonucleotideA$^{5'}$-LR(LR)$_3$G-CONH$_2$	100	100±3
P4G-A-CONH$_2$	$^{3'}$OligonucleotideA$^{5'}$-LRLRG(LR)$_2$G-CONH$_2$	100	97±2

Figure 7. Cleavage of 3′-FITC-tRNA^{Phe} with peptidyl−oligonucleotide conjugates P2-A-COOH, P4-A-COOH, and P4-A-CONH$_2$. A. Representative images of 12% PAA/8 M urea gel after electrophoresis of 3′-FITC-tRNA^{Phe} cleavage products. Lanes T1 and Im, partial RNA digestion with RNase T1 and imidazole ladder, respectively. Lane C, RNA incubated without conjugates for 24 h. tRNA^{Phe} (at 1 μM concentration) was incubated with the conjugates at concentration 20 μM at 37 °C for different times. Positions of RNA cleavage with conjugates and RNase T1 are shown on the right and left, respectively. B. Kinetics of 3′-FITC-tRNA^{Phe} cleavage at 37 °C and conjugate concentration 20 μM. C. Conjugate structure, binding, and cleavage extent.

tRNA:conjugate ratio (POC:tRNA^{Phe}, 7:1) is approximately 70%. The fact that cleavage is below 97 ± 8% (observed at the cleavage plateau, above 20 μM conjugate concentration) could be attributed to binding representing an equilibrium process with the possibility for the conjugate to temporarily dissociate from the POC:tRNA^{Phe} complex. At higher P4G-A-COOH concentrations, the binding equilibrium is shifted in favor of the heteroduplex and higher cleavage activities (97%) are observed.

Cleavage Activity of Conjugates: Kinetics. To evaluate the effect of various structural alterations in the catalytic peptide on catalytic activity and sequence-selectivity of peptidyl−oligonucleotide conjugates, we assessed four different structural variants of P4G-A-COOH against tRNA^{Phe} (i.e., P2-A-COOH, P4-A-COOH, P4-A-CONH$_2$, and P4G-A-CONH$_2$). Kinetic experiments were carried out for all five POC structural variants (including P4G-A-COOH) to elucidate the time dependence of RNA cleavage with an excess of each conjugate against FITC-tRNA^{Phe} (POC:tRNA^{Phe}, 20:1, 20 μmol L^{-1}) over a 24 h period (Figure 7). These correspond to single-turnover reaction conditions and thus provide reliable kinetic data for comparisons of cleavage activity of POCs, as the hybridization proceeds similarly over the concentration range. P2-A-COOH shows minimal RNA cleavage level (up to 7%) during this time frame, with the major cut at U8-A9, a position adjacent to the junction, and faint cleavage at C63-A64 linkage within the target site. P4-A-COOH displays moderate cleavage activity (up

DOI: 10.1021/acs.bioconjchem.5b00193
Bioconjugate Chem. 2015, 26, 1129−1143

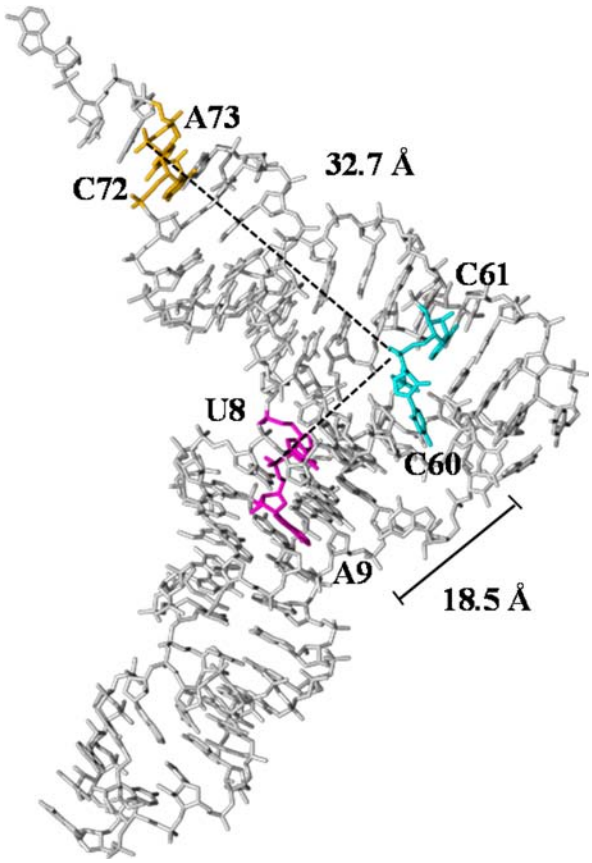

Figure 8. Crystal structure of $tRNA^{Phe}$[54] showing distances (dotted lines) between (site opposite) attachment point of peptide (C60-p-C61, cyan) and distant cleavage sites U8-p-U9 (magenta) and C72-p-A73 (yellow).

to 24%) with the plateau level reached after 8 h of reaction. This POC cleaves tRNA at three sites with intensities of cleavage decreasing in order U8-A9 > C63-A64 ≥ C73-A74. In contrast, POCs P4G-A-COOH, P4-A-$CONH_2$, and P4G-A-$CONH_2$ show a high level of cleavage activity (up to 100%) over 24 h, reaching a plateau between the 4 and 8 h time points (Figure 7A,B). This extent of cleavage is far superior to that previously demonstrated for a structurally similar POC targeting the TΨC loop of $tRNA^{Lys}$ at 100-fold excess of conjugate over RNA target (55% over 24 h at a POC:$tRNA^{Lys}$ ratio of 100:1).[7] Cleavage sites were attributed to the U8-A9, C63-A64, and C72-A73 positions. Accumulation of the tRNA cleavage products corresponding to each particular site occurs with different kinetics. The U8-A9 band increases in intensity up to the 1 h time point and then levels off. The reduction in the intensity of this band over time is presumably due to additional cleavage of this fragment occurring. The delay in the cleavage between sites C63-A64 (located in the TΨC stem) and C72-A73 (located in the acceptor stem) suggests that the latter is in fact a secondary cleavage event. This may be tentatively due to a structural rearrangement of the $tRNA^{Phe}$ following cleavage at C63-A64, placing the peptide cleaving group closer to C72-A73 in the acceptor stem than it appears to be in the intact $tRNA^{Phe}$ secondary structure.

The experimentally observed cut within the additional U8-A9 site, which is located on the edge of the D-arm, may also result from sequence-specific cleavage, presumably due to the close proximity of this region to the target sequence within the TΨC-arm of the $tRNA^{Phe}$ tertiary structure. Indeed, unique tertiary interactions between the D- and TΨC-loops, which are maintained by the G18-Ψ55 and G19-C56 base-paring, hold D- and TΨC-loops together, thus contributing to formation of the "L-shaped" tertiary structure of tRNA. Analysis of the available X-ray structure[54] of the yeast $tRNA^{Phe}$ using YASARA NOVA[55] software (see Figure 8) showed that the distance between the bridging phosphorus atoms of C60-p-C61 (i.e., the region in the TΨC-arm opposite to the attachment point of the catalytic peptide) and the U8-p-A9 fragment was only 18.5 Å. The maximum length of the unfolded peptides P4G and P4 measured using YASARA software was found to be 36.5 and 32.8 Å, respectively, thus implying that, even in this conformationally restricted tertiary $tRNA^{Phe}$ structure (stabilized by Mg^{2+} ions), the site (U8-p-A9) can be potentially reached by catalytic peptide to achieve successful cleavage. In the absence of Mg^{2+} ions and with partially unfolded TΨC-arm after hybridization with the POC, the tertiary structure of tRNA becomes more conformationally flexible, thus enhancing the opportunity for the catalytic peptide to reach these relatively distant sites.

Another (additional) cleavage site (C72-A73) seems to be located more distantly from the "anchor" C60-C61 region. The distance between the bridging phosphorus atoms of the C60-p-C61 and C72-p-A73 sites was found to be 32.7 Å. Again, this cleavage site is within reach of P4G and P4 in their unfolded conformations (see Figure 6). The importance of the tRNA structural flexibility on overall cleavage output is highlighted by our cleavage experiments carried out in the presence of Mg^{2+} ions (see also discussion below), which clearly demonstrated that restriction of conformational flexibility had a detrimental effect on cleavage efficiency, which was more profound for relatively distant cleavage sites (e.g., U8-A9). In contrast, an increase in structural flexibility of tRNA can allow even the shorter peptide P2-COOH (maximum length of 18.2 Å) to reach the U8-A9 (but not C72-A73) site when incorporated into the P2-A-COOH conjugate, although its cleavage efficiency was considerably lower as compared with that seen for the P4G and P4 peptides (cf., P2-A-COOH with P4-A-COOH, P4-A-$CONH_2$, PG4-A-COOH, and PG4-A-$CONH_2$) on Figures 6 and 7.

Structure−Activity Relationships. Kinetic experiments revealed the sharp differences between the cleavage activities of POCs only slightly differing in the structure of the catalytic peptide. Addition of a glycine residue between two $(LR)_2$ motives significantly (by a factor of 4) increases the cleaving activity of the conjugate (cf., P4-A-COOH (24 ± 3%) and P4G-A-COOH (97 ± 8%), Figure 7B; plateau points at 24 h). Similarly, replacement of the C-terminal carboxylic acid group in P4-A-COOH with a carboxamide group to produce P4-A-$CONH_2$ also results in a 4-fold increase (from 24 ± 3% to 100 ± 3%) in cleavage activity of POC (cf., P4-A-COOH and P4-A-$CONH_2$, Figure 7A,B). Notably, analogous replacement of the C-terminal −COOH group with a $-CONH_2$ group in P4G-A-COOH to generate P4G-A-$CONH_2$ (97 ± 2%) practically did not change (within the experimental error) the cleavage activity of the former conjugate, which already showed maximum of cleavage activity (97 ± 8%). It looks possible that in the latter case the optimal catalytic structure of the peptide is formed regardless of the specific functional group present at the peptide C-terminus, presumably due to the presence of an extra glycine residue in the middle of the peptide chain. Reaction half-lives calculated from the kinetic data are 35, 45, and 53 min for P4-

DOI: 10.1021/acs.bioconjchem.5b00193
Bioconjugate Chem. 2015, 26, 1129−1143

A-$CONH_2$, P4G-A-$CONH_2$, and P4G-A-COOH, respectively. It is worth mentioning that the observed significant increase in cleavage activity of P4-A-$CONH_2$ cannot be explained alone by reduction of charge repulsion; it is more likely that the $-CONH_2$ group contributes to the catalysis of phosphodiester transesterification reaction.

The mechanism of guanidinium-mediated RNA cleavage is only partly understood; however, the nature of the guanidinium−phosphate interaction is well reported.[35,36,56] The active sites of various phosphodiester cleaving enzymes (e.g., Staphylococcal nuclease,[57] Ribonuclease A,[58] Ribonuclease T1,[59] Phospholipase C[58]) contain arginine residues which have been implicated in (i) stabilizing the phosphorane transition state, (ii) assisting the delivery of the negatively charged 2′-oxygen to the phosphorus, as well as (iii) acting as general-acid catalysts.[56] In our system, it could be postulated that the arginine residues would form similar guanidinium-phosphate/phosphorane contacts to achieve RNA cleavage. The observed increase in RNA cleavage activity for P4-A-$CONH_2$ over P4-A-COOH could be attributed to the presence of the additional hydrogen bond donors which may be able to form similar stabilizing contacts with the phosphate groups. The insertion of an additional glycine residue may improve this process further by enhancing the conformational freedom of the peptide, thus allowing the POCs to explore more energetically favorable conformations, which could be optimal for the interactions with the RNA backbone.

Similar variations in tRNA cleavage activities have already been reported for a noncomplementary class of POCs containing the same tetrathymidylate (T_4) oligodeoxynucleotide fragment and subtly different peptide sequences.[60] For example, POCs containing the peptide $(LR)_n$-G-NH_2 (n = 2 or 4) cleaved a 96-nucleotide HIV-1 RNA (G-X motifs only) at 25% and 45%, respectively, whereas only negligible cleavage activity was observed for a similar peptide when n = 3. Additionally, replacement of a single leucine with a proline residue (when n = 4) diminished cleavage activity (~5%) and changed the cleavage specificity from G-X to Pyr-A motifs. Conjugates bearing only arginine-containing peptide (R_5-T_4) and the serine-arginine containing peptide (S_2R_3-T_4) also had faint ribonuclease activity when conjugated to T_4, thus emphasizing the importance of the regular (-LR-) blocks and additional interactions provided by the more hydrophobic leucine. It is clear, therefore, that peptide structural properties are crucial for RNA cleavage activity: amino acid sequence, peptide length, charge separation, sequence regularity, secondary structure, and overall conformational flexibility appear to play a significant role in catalytic performance. However, to fully evaluate the rules that govern these catalytic activities, three-dimensional structures of the POC:$tRNA^{Phe}$ heteroduplexes would need to be obtained from a combination of high-field multidimensional NMR experiments, X-ray crystallography, and molecular modeling, all of which are beyond the scope of this paper.

Controls of Cleavage Specificity. Competition experiments were performed to confirm the sequence-specific manner of $tRNA^{Phe}$ cleavage with POCs (see Supporting Information). To this end, the cleavage reaction with P4G-A-COOH (5 μM) was performed in the presence of parent oligonucleotide **A** (50 μM) and oligonucleotide **B** (50 μM) complementary to the sequence (60−76). As expected, the reaction was suppressed by oligonucleotide **A**, while oligonucleotide **B** entirely abolished cleavage at the C63-A64 and C73-A74 sites by forming a duplex with the target sequence. Cleavage at the U8-A9 site however was still observed.

To prove the affinity character of the cleavage, the reaction was performed in the presence of magnesium ions, which are known to significantly stabilize the $tRNA^{Phe}$ secondary and tertiary structure. Stabilization of tRNA structure in the presence of 5 mM $MgCl_2$ alters both the specificity and kinetics of $tRNA^{Phe}$ cleavage by P4G-A-COOH (see Supporting Information). Under these conditions, cleavage at U8-A9 linkage is entirely abolished, while cleavage at C63-A64 site becomes predominant with the secondary cleavage event occurring at C73-A74. A similar increase of cleavage selectivity upon structure stabilization was observed previously for Influenza virus M2 RNA.[49] Thus, stabilization of $tRNA^{Phe}$ structure increases specificity of cleavage. This result confirms that cleavage of the U8-A9 site occurs in a sequence specific manner as a result of the flexibility of this $tRNA^{Phe}$ region upon POC binding with the complementary sequence and subsequent rearrangement of the TΨC-arm, rather than due to the flexibility of the catalytic peptide. Stabilization of the $tRNA^{Phe}$ structure by Mg^{2+} slows down RNA cleavage (40% at 25 h time point) with the plateau not achieved at the 25 h time point.

As a control for the specificity of cleavage, a 3′-FITC-HIV RNA was used containing no homology with $tRNA^{Phe}$ (see Supporting Information). Cleavage of this RNA was absent with P4G-A-COOH (20 μM) except for some cuts (less than 5%) in the incubation control (with no POC added) and at time points 30 min and 4 h, which do not reproduce at other time points and can be attributed to a spontaneous RNA cleavage upon probe manipulations prior to electrophoresis.

Diethylpyrocarbonate (DEPC) treatment confirms that the $tRNA^{Phe}$ cleavage observed in the presence of POCs is the result of a POC catalyzed transesterification reaction (see Supporting Information). Incubation of the conjugates under the conditions of RNase A inactivation (or other RNase contaminants) has no effect on the level of $tRNA^{Phe}$ cleavage or specificity, thus confirming that the observed degradation of the target RNA is fully attributed to the catalytic activity of this type of chemical ribonucleases.

CONCLUSION

A small library of POCs (i.e., P4G-A-COOH, P2-A-COOH, P4-A-COOH, P4-A-$CONH_2$, and P4G-A-$CONH_2$) have been designed and synthesized, some of which demonstrated effective (up to 100%) site-selective cleavage of $tRNA^{Phe}$. A combination of C-terminal peptide functionality and/or peptide flexibility via a central glycine residue proves to be integral to tRNA cleavage efficiency. A 6-fold increase in RNA cleavage activity was observed upon switching from a C-terminal carboxylic acid to a C-terminal carboxamide peptide for the P4-A-type of conjugates, while a more subtle increase (~10%) was observed for the P4G-A-type conjugate upon similar modification. The nature of the cleavage patterns observed are indicative of the POCs targeting the desired ^{61}CACAG^{65} site in the TΨC stem region in a 1:1 fashion. However, due to the increased flexibility of the TΨC loop region upon hybridization and the length of the peptides, additional cleavage sites (U8-A9, C73-A74) were also observed.

Quantitative cleavage of $tRNA^{Phe}$ by P4-A-$CONH_2$ conjugate observed over a 24 h period demonstrates that POCs could be used as the basis to generate tools for gene-silencing and antiviral therapeutics. In addition, the POCs described here do

DOI: 10.1021/acs.bioconjchem.5b00193
Bioconjugate Chem. 2015, 26, 1129−1143

not require any additional cofactors or enzymes. POCs have been shown here (and in previous work) to preferentially cleave CpA and UpA motifs within single-stranded RNA regions,[7−9,50,60] which are ubiquitous in mammalian and viral RNAs. However, the directed sequence selectivity of developed POCs means that the RNA cleavage will be directed by the recognition (i.e., oligonucleotide) element, which is designed to find the complementary region of the target RNA and hybridize to it via specific Watson−Crick hydrogen bonding. In the intricate human genome, any sequence of 17 bases is expected to occur only once; however, due to the nonrandom nature of mammalian RNA an oligonucleotide containing fewer bases could bind exclusively to its complementary RNA sequence.[61−63] By using RNA structure prediction programs (e.g., Mfold, RNAfold, RNAstructure), it is possible to identify hairpin and loop regions within disease-relevant RNAs which fulfill the hybridization and cleavage criteria and are suitable for targeting with short oligodeoxynucleotide sequences and hence POCs. Literature examples of previous artificial ribonuclease targets include the following: HIV Rev Response Element;[50] 96-mer HIV-1 TAR RNA;[64] HIV-1 gagRNA;[13] Human c-raf-1 mRNA;[28] $tRNA^{Lys}$.[7]

Peptidyl−oligonucleotide conjugates have been shown to induce efficient cleavage of RNA sequences leading to irreversible damage of biologically significant RNA targets. At one extreme, direct site-specific cleavage without significant catalytic amplification was observed for complementary RNA targets (demonstrated in this research). At the other extreme, efficient cleavages with high catalytic turnover can be achieved in poorly complementary RNA regions.[8,9] In order for this class of bioconjugates to be clinically beneficial, potency must be increased to a level where the concentration of POC required for RNA cleavage is within means of being realized in a cellular environment, i.e., substoichiometric. Our next challenge therefore is to combine sequence specificity with high catalytic turnover. In this case, the POCs could act like enzyme mimics by turning over multiple RNA substrates.

MATERIALS AND INSTRUMENTS

Chemicals and solvents were purchased from Sigma-Aldrich (UK) unless otherwise stated. T7 RNA polymerase was a generous gift of Dr. S. Khodyreva (Institute of Chemical Biology and Fundamental Medicine SB RAS). Bst2UI and Fok1 restriction endonucleases were from Sibenzyme. RNase T1 was from Fermentas. p67YF90 was a generous gift of Dr. N. Moor (Institute of Chemical Biology and Fundamental Medicine SB RAS). pHIV-1 was a generous gift of Prof. H. J. Gross (Chair of Biochemistry, Biocenter, University of Würzburg, Germany). All buffers were prepared using Milli-Q water and were filtered through 0.22 μM membrane. All chemicals used were of analytical grade and used without further purification. Custom oligonucleotides were purchased from AtdBio Ltd. (Southampton, UK). Fmoc-Gly-Rink Amide-MBHA (0.42 mmol/g) peptide resin was purchased from Eurogentec Ltd. (Southampton, UK). Water was purified in-house via a Milli-Q purification system (Millipore, USA). HPLC purifications of product peptides and conjugates were carried out on an Agilent 1100 HPLC system (Agilent Technologies, Santa Clara, CA) consisting of a diode array detector (set to λ = 220 or 260 nm, respectively), Rheodyne (3725i) manual injector, and a Luna C18(2) (250 × 10 mm, 100 Å pore size, Phenomenex; CA, USA) reverse-phase semipreparative column. ESI mass spectral data was collected on a Thermo Scientific LTQ Orbitrap XL (MA, USA) at the EPSRC National Mass Spectrometry Facility, (Swansea, UK). MALDI (matrix-assisted laser desorption ionization) mass spectral data was collected on a Bruker Daltonics Ultraflex TOF/TOF mass spectrometer (MA, USA), at the Manchester Interdisciplinary Biocenter, University of Manchester. Analysis of POCs by MALDI was achieved with the THAP (2,4,6-trihydroxyacetophenone monohydride) (25 mg/mL) matrix with the addition of ammonium citrate (5 mg/mL), 50% AcCN, and 0.1% TFA. Ions were only observed in positive mode as either (di)sodium or potassium adducts. Notably, other matrices, α-cyano-4-hydroxycinnamic acid, sinapinic, and 3-hydroxypicolinic acid failed to yield molecular ion peaks in either positive or negative ionization modes. ^{1}H and ^{31}P NMR (nuclear magnetic resonance) spectra were collected on a Bruker Avance II+ 400 Ultrashield spectrometer (MA, USA). ^{13}C NMR spectra were collected on a Bruker Avance 300 spectrometer (MA, USA). The software *Topspin 3.2* was used to analyze the NMR data obtained. A Kaiser test was used to visualize Fmoc deprotection and successful amino acid coupling. This consisted of incubating approximately 1 mg of peptide resin with Ninhydrin solution (50 μL) (1.5 g ninhydrin, 5 mL acetic acid, 500 mL 95% ethanol) and piperidine (50 μL) at 120 °C for 5 min.

EXPERIMENTAL PROCEDURES

Peptide Synthesis. Peptides (P4-COOH, P4-$CONH_2$, P4G-COOH, P4G-$CONH_2$, P2-COOH) were synthesized by manual solid-phase methodology on either an Fmoc-Gly-Wang resin (250 mg, 0.2 mmol) or a Fmoc-Gly-Rink Amide-MBHA resin (215 mg, 0.18 mmol) using the Fmoc/^{t}Bu strategy. Fmoc deprotections were achieved with 20% piperidine in DMF solution for 30 min at room temperature (RT). Between each synthetic step, resin washings were carried out with DMF (2 × 10 mL), DCM (2 × 10 mL), and DMF (2 × 10 mL).

Wang Resin. Amino acid couplings were achieved by preactivating Fmoc-Leu-OH (212 mg, 0.6 mmol); Fmoc-Gly-OH (178 mg, 0.54 mmol); or Fmoc-Arg(Pbf)-OH (389 mg, 0.6 mmol) in DMF (10 mL) with HBTU (220 mg, 0.58 mmol) and DIPEA (122 μL, 0.7 mmol).

MBHA Resin. Amino acid couplings were achieved by preactivating Fmoc-Leu-OH (191 mg, 0.54 mmol); Fmoc-Gly-OH (161 mg, 0.54 mmol); or Fmoc-Arg(Pbf)-OH (352 mg, 0.54 mmol) in DMF (10 mL) with HBTU (198 mg, 0.52 mmol) and DIPEA (110 μL, 0.63 mmol). Once added to the resins, the reactions proceeded at RT for 30 min under mechanical shaking. Successful Fmoc deprotection/amino acid coupling could be visualized by carrying out a Kaiser test. Following completion of the sequence, the peptide was cleaved from the resin by shaking with TFA/TIPS/H_2O (95/2.5/2.5) (15 mL) at RT for 3 h. The volume of the resulting solution was reduced by 2/3, pipetted into cold (−20 °C) TBME and stored at −20 °C overnight. The precipitate was collected by centrifugation (4000 rpm, 5 min, 4 °C) and the resulting pellets were washed with cold TBME (2 × 10 mL) and isolated by centrifugation. Once air-dry, the pellets were solubilized in acetonitrile/water/TFA (40/60/0.1) and freeze−dried.

Peptide Purification. Crude lyophilized peptides were solubilized in 30% acetic acid and purified using RP-HPLC. The flow rate was maintained at 1.5 mL/min using 0.1% TFA/water as eluent A and 0.1% TFA/AcCN as eluent B. The absorbance was monitored at 220 nm and the following gradients were applied: 15% B for 1 min, 15% B to 37% B in 34 min for peptides **1** and **3**; 10% B for 1 min, 10% B to 30% B in

DOI: 10.1021/acs.bioconjchem.5b00193
Bioconjugate Chem. 2015, 26, 1129−1143

40 min for peptides **2** and **4**; 100% A for 1 min, 0% to 35% B over 35 min for peptide **5**.

*NH_2-LRLRGLRLRG-$CONH_2$ (P4G-$CONH_2$) (**1**).* Fractions at 22 min were collected, combined, and lyophilized to yield the TFA salt of **1** as a fluffy white material (203 mg, 63%). ESI-MS: m/z = 604.9 for $[M+2H]^{2+}$, 304.2 for $[M+3H]^{3+}$ (MW = 1207.81 calcd. for $[C_{52}H_{101}N_{23}O_{10}]$). ^{1}H NMR ($D_2O$ with TSP (0.1 μM), 400 MHz): δ 0.82−0.91 (m, 24H, Leu-H$^{\delta}$), 1.49−1.88 (m, 28H, 8 × Arg-H$^{\delta}$, 8 × Arg-H$^{\gamma}$, 8 × Leu-H$^{\beta}$, 4 × Leu-H$^{\gamma}$), 3.14−3.18 (m, 8H, Arg-H$^{\beta}$), 3.88 (m, 4H, Gly-H), 3.97 (t, 1H, J = 7.36 Hz, N-Leu-H$^{\alpha}$), 4.24−4.39 (m, 7H, Leu/Arg-H$^{\alpha}$).

*NH_2-LRLRGLRLRG-COOH (P4G-COOH) (**2**).* Fractions at 36 min were collected, combined, and lyophilized to yield the TFA salt of **2** as a fluffy white material (260 mg, 73%). ESI-MS: m/z = 1209.8 for $[M + H]^+$ (MW = 1208.79 calcd. for $[C_{52}H_{100}N_{22}O_{11}]$). ^{1}H NMR ($D_2O$ with TSP (0.1 μM), 400 MHz): δ 0.81−0.90 (m, 24H, Leu-H$^{\delta}$), 1.49−1.88 (m, 28H, Leu-H$^{\beta,\gamma}$, Arg-H$^{\gamma,\delta}$), 3.15 (s, 8H, Arg-H$^{\beta}$), 3.80−3.91 (m, 4H, Gly-H), 3.97 (t, 1H, J = 7.56 Hz, N-Leu-H$^{\alpha}$), 4.26−4.38 (m, 7H, Leu/Arg-H$^{\alpha}$).

*NH_2-LRLRLRLRG-$CONH_2$ (P4-$CONH_2$) (**3**).* Fractions at 24 min were collected, combined, and lyophilized to yield the TFA salt of **3** as a fluffy white material (214 mg, 69%). ESI-MS: m/z = 576.4 for $[M+2H]^{2+}$, 384.6 for $[M+3H]^{3+}$ (MW = 1150.79 calcd. for $[C_{50}H_{98}N_{22}O_9]$). ^{1}H NMR (D_2O with TSP (0.1 μM), 400 MHz): δ 0.89−0.95 (m, 24H, Leu-H$^{\delta}$), 1.55−1.91 (m, 28H, 8 × Arg-H$^{\delta}$, 8 × Arg-H$^{\gamma}$, 8 × Leu-H$^{\beta}$, 4 × Leu-H$^{\gamma}$), 3.22 (s, 8H, Arg-H$^{\beta}$), 3.93 (m, 2H, Gly-H), 3.99 (m, 1H, N-Leu-H$^{\alpha}$), 4.34−4.43 (m, 7H, Leu/Arg-H$^{\alpha}$).

*NH_2-LRLRLRLRG-COOH (P4-COOH) (**4**).* Fractions at 40 min were collected, combined, and lyophilized to yield the TFA salt of **4** as a fluffy white material (245 mg, 71%). ESI-MS: m/z = 598.9 for $[M+2Na]^{2+}$, 384.9 for $[M+3H]^{3+}$ (MW = 1151.77 calcd. for $[C_{50}H_{97}N_{21}O_{10}]$). ^{1}H NMR ($D_2O$ with TSP (0.1 μM), 400 MHz): δ 0.87−0.97 (m, 24H, Leu-H$^{\delta}$), 1.53−1.93 (m, 28H, 8 × Arg-H$^{\delta}$, 8 × Arg-H$^{\gamma}$, 8 × Leu-H$^{\beta}$, 4 × Leu-H$^{\gamma}$), 3.18−3.23 (m, 8H, Arg-H$^{\beta}$), 3.86−4.05 (m, 3H, 2 × Gly-H, 1 × N-Leu-H$^{\alpha}$), 4.31−4.43 (m, 7H, Leu/Arg-H$^{\alpha}$).

*NH_2-LRLRG-COOH (P2-COOH) (**5**).* Fractions at 32 min were collected, combined and lyophilized to yield the TFA salt of **5** as a fluffy white material (120 mg, 63%). ESI-MS: m/z = 614.4 for $[M + H]^+$, 307.7 for $[M + H]^{2+}$ (MW = 613.40 calcd. for $[C_{26}H_{51}N_{11}O_6]$). ^{1}H NMR (D_2O with TSP (0.1 μM), 400 MHz): δ 0.87−0.95 (m, 12H, Leu-H$^{\delta}$), 1.56−1.94 (m, 14H, 4 × Arg-H$^{\delta}$, 4 × Arg-H$^{\gamma}$, 4 × Leu-H$^{\beta}$, 2 × Leu-H$^{\gamma}$), 3.18−3.23 (m, 4H, Arg-H$^{\beta}$), 3.89 (d, J = 8.28 Hz, 2H, Gly-H), 4.01 (t, J = 6.72 Hz, 1H, N-Leu-H$^{\alpha}$), 4.33−4.43 (m, 3H, Leu/Arg-H$^{\alpha}$).

Conjugate Synthesis (Carboxamide Peptides 1 and 3). 5′-Phosphate modified oligonucleotide, pGATCGAACACAGGACCT (Oligonucleotide **A**) (0.12 μmol) in H_2O (100 μL) was converted into a DMSO soluble salt through multiple (10 μL) additions of a 4% (w/v) cetyltrimethylammonium bromide solution. After each subsequent addition, the solution was centrifuged (13 400 rpm, 4 min). After oligonucleotide **A** precipitation stopped, the pellet was washed with H_2O (2 × 500 mL) and freeze−dried. Following drying, the pellet was solubilized in anhydrous DMSO (50 μL). To this was added an excess of triphenylphosphine (10 mg, 38 μmol), 2,2′-dipyridyl disulfide (10 mg, 45 μmol), and 4-(dimethylamino)pyridine (5 mg, 41 μmol). Anhydrous DMSO (20 μL) and 4-(dimethylamino)pyridine (3 mg, 25 μmol) were added to either P4G-$CONH_2$ (**1**) (1.2 μmol) or P4-$CONH_2$ (**3**) (1.2 μmol), and the resulting solution was added directly to the oligonucleotide **A** solution and incubated at 40 °C for 3 h. 4% $LiClO_4$ in acetone (w/v) (1.8 mL) was added and the reaction mixture left at −80 °C overnight. After centrifugation (13 400 rpm, 4 min) the supernatant was discarded and the pellet left to air-dry. The dry pellet was vortexed vigorously with 3 M $LiClO_4$ (120 μL) and centrifuged (13 400 rpm, 4 min). The supernatant was carefully transferred into 4% $LiClO_4$ in acetone (w/v) (1.8 mL) and kept at −80 °C for 3 h. Following centrifugation (13 400 rpm, 4 min) the supernatant was discarded and the pellet left to air-dry before HPLC purification.

Conjugate Synthesis (Carboxylic Acid Peptides 2, 4, and 5). 5′-Phosphate modified oligonucleotide, pGATCGAACACAGGACCT (Oligonucleotide **A**) (0.12 μmol) in H_2O (100 μL) was converted into a DMSO soluble salt through multiple (10 μL) additions of a 4% (w/v) cetyltrimethylammonium bromide solution. After each subsequent addition, the solution was centrifuged (13 400 rpm, 4 min). After oligonucleotide **A** precipitation stopped, the pellet was washed with H_2O (2 × 500 mL) and freeze−dried. Following drying, the pellet was solubilized in anhydrous DMSO (50 μL). To this was added an excess of triphenylphosphine (10 mg, 38 μmol), 2,2′-dipyridyl disulfide (10 mg, 45 μmol), and 4-(dimethylamino)pyridine (5 mg, 41 μmol). The solution was incubated at 40 °C for 30 min. 1.8 mL anhydrous diethyl ether was added and the reaction mixture left at −80 °C for 1 h. After centrifugation (13 400 rpm, 4 min) the supernatant was discarded and the pellet left to air-dry. The pellet containing activated oligonucleotide **A** was then solubilized in DMSO (70 μL) containing 4-(dimethylamino)-pyridine (3 mg, 25 μmol) and peptide (1.2 μmol): P4G-COOH (**2**), P4-COOH (**4**), or P2-COOH (**5**). The resulting solution was added incubated at 40 °C for 3 h. 4% $LiClO_4$ in acetone (w/v) (1.8 mL) was added and the reaction mixture left at −80 °C overnight. After centrifugation (13 400 rpm, 4 min) the supernatant was discarded and the pellet left to air-dry. The dry pellet was vortexed vigorously with 3 M $LiClO_4$ (120 μL) and centrifuged (13 400 rpm, 4 min). The supernatant was carefully transferred into 4% $LiClO_4$ in acetone (w/v) (1.8 mL) and kept at −80 °C for 3 h. Following centrifugation (13 400 rpm, 4 min) the supernatant was discarded and the pellet left to air-dry before HPLC purification.

Conjugate Purification. Crude conjugates were dissolved in 0.05 M $LiClO_4$ and purified using RP-HPLC. The flow rate was maintained at 2.0 mL/min using 0.05 M $LiClO_4$ as eluent A and 0.05 M $LiClO_4$ in AcCN as eluent B. The absorbance was monitored at 260 nm and the following gradient was applied: 100% A for 3 min, 0% B to 40% B in 27 min for conjugates **6**, **7**, **8**, and **9**; 100% A for 3 min 0% B to 18% B in 32 min for conjugate **10**.

*P4G-A-COOH (**6**).* Fractions at 21 min were collected, combined, and lyophilized. The excess salt was removed by dissolving the material in H_2O (100 μL) and precipitating in 4% $LiClO_4$ in acetone (w/v) (1.8 mL) overnight. The product was collected by centrifugation (13400 rpm, 4 min), air-dried and then freeze−dried to give a white powder (8.6 nmol, 72%). MALDI-MS: m/z = 3254 $[M+Na+Na]^{2+}$, 6503 for $[M+ACN+H]^+$ (MW = 6461 calcd. for $[C_{217}H_{311}N_{91}O_{109}P_{17}]$). ^{1}H NMR ($D_2O$ with TSP (0.01 μM), 400 MHz): δ 0.64−0.86 (m, 24H, Leu-H$^{\delta}$), 1.08−2.76 (m, 68H, 17 × H2′ and 17 × H2″ sugar ring protons, 2 × CH_3 of 2 × dT, 8 × Arg-H$^{\delta}$, 8 × Arg-H$^{\gamma}$, 8 × Leu-H$^{\beta}$, 4 × Leu-H$^{\gamma}$), 3.01−3.15 (m, 8H, 8 × Arg-H$^{\beta}$), 5.46−

DOI: 10.1021/acs.bioconjchem.5b00193
Bioconjugate Chem. 2015, 26, 1129−1143

6.29 (m, 22H, 17 × H1′ sugar ring protons, 5 × H5 of dC), 7.25−8.28 (m, 23H, 23 × Ar−H from dG (×4), dA (×12), dC (×5), and dT (×2). The H3′/H4′/H5′/H5″ sugar ring proton regions (3.5−5.0 ppm) were not analyzed due to suppression of residual water signal at 4.8 ppm. $^{31}P\{^1H\}$ NMR (D_2O, 160 MHz): δ −1.44 to −0.78 (16P, $\underline{P}O_4$), 5.88 (1P, N-$\underline{P}O_3$). No sample reference was used for ^{31}P NMR analysis. It was carried out to observe the relative shift of the ^{31}P−N resonance.

*P4G-A-CONH$_2$ (**7**).* Fractions at 22 min were collected, combined, and lyophilized. The excess salt was removed by dissolving the material in H_2O (100 μL) and precipitating in 4% $LiClO_4$ in acetone (w/v) (1.8 mL) overnight. The product was collected by centrifugation (13400 rpm, 4 min), air-dried, and then freeze−dried to give a white powder (10.3 nmol, 86%). MALDI-MS: m/z = 3252 $[M+Na+Na]^{2+}$, 6482 $[M + Na]^+$ (MW = 6459 calcd. for $[C_{217}H_{311}N_{92}O_{108}P_{17}]$). ^1H NMR (D_2O with TSP (0.01 μM), 400 MHz): δ 0.70−0.87 (m, 24H, Leu-H$^{\delta}$), 1.17−2.80 (m, 68H, 17 × H2′ and 17 × H2″ sugar ring protons, 2 × CH_3 of 2 × dT, 8 × Arg-H$^{\delta}$, 8 × Arg-H$^{\gamma}$, 8 × Leu-H$^{\beta}$, 4 × Leu-H$^{\gamma}$), 3.08−3.18 (m, 8H, 8 × Arg-H$^{\beta}$), 5.53−6.36 (m, 22H, 17 × H1′ sugar ring protons, 5 × H5 of dC), 7.32−8.35 (m, 23H, 23 × Ar−H from dG (×4), dA (×12), dC (×5), and dT (×2). The H3′/H4′/H5′/H5″ sugar ring proton regions (3.5−5.0 ppm) were not analyzed due to suppression of residual water signal at 4.8 ppm. $^{31}P\{^1H\}$ NMR (D_2O, 160 MHz): δ −1.60 to −0.86 (16P, $\underline{P}O_4$), 5.84 (1P, N-$\underline{P}O_3$). No sample reference was used for ^{31}P NMR analysis. It was carried out to observe the relative shift of the ^{31}P−N resonance.

*P4-A-COOH (**8**).* Fractions at 22 min were collected, combined, and lyophilized. The excess salt was removed by dissolving the material in H_2O (100 μL) and precipitating in 4% $LiClO_4$ in acetone (w/v) (1.8 mL) overnight. The product was collected by centrifugation (13400 rpm, 4 min), air-dried, and then freeze−dried to give a white powder (8.5 nmol, 71%). MALDI-MS: m/z = 3211 $[M+H+Na]^{2+}$, 6424 $[M + Na]^+$ (MW = 6401 calcd. for $[C_{215}H_{304}N_{90}O_{108}P_{17}]$). ^1H NMR (D_2O with TSP (0.01 μM), 400 MHz): δ 0.62−0.86 (m, 24H, Leu-H$^{\delta}$), 1.09−2.74 (m, 68H, 17 × H2′ and 17 × H2″ sugar ring protons, 2 × CH_3 of 2 × dT, 8 × Arg-H$^{\delta}$, 8 × Arg-H$^{\gamma}$, 8 × Leu-H$^{\beta}$, 4 × Leu-H$^{\gamma}$), 3.03−3.12 (m, 8H, 8 × Arg-H$^{\beta}$), 5.46−6.28 (m, 22H, 17 × H1′ sugar ring protons, 5 × H5 of dC), 7.24−8.29 (m, 23H, 23 × Ar−H from dG (×4), dA (×12), dC (×5), and dT (×2). The H3′/H4′/H5′/H5″ sugar ring proton regions (3.5−5.0 ppm) were not analyzed due to suppression of residual water signal at 4.8 ppm. $^{31}P\{^1H\}$ NMR (D_2O, 160 MHz): δ −1.38 to −1.05 (16P, $\underline{P}O_4$), 5.82 (1P, N-$\underline{P}O_3$). No sample reference was used for ^{31}P NMR analysis. It was carried out to observe the relative shift of the ^{31}P−N resonance.

*P4-A-CONH$_2$ (**9**).* Fractions at 24 min were collected, combined, and lyophilized. The excess salt was removed by dissolving the material in H_2O (100 μL) and precipitating in 4% $LiClO_4$ in acetone (w/v) (1.8 mL) overnight. The product was collected by centrifugation (13 400 rpm, 4 min), air-dried, and then freeze−dried to give a white powder (10.6 nmol, 88%). MALDI-MS: m/z = 3213 $[M+H+Na]^{2+}$, 6441 $[M+K]^+$ (MW = 6402 calcd. for $[C_{215}H_{304}N_{91}O_{107}P_{17}]$). ^1H NMR (D_2O with TSP (0.01 μM), 400 MHz): δ 0.68−0.87 (m, 24H, Leu-H$^{\delta}$), 1.29−2.85 (m, 68H, 17 × H2′ and 17 × H2″ sugar ring protons, 2 × CH_3 of 2 × dT, 8 × Arg-H$^{\delta}$, 8 × Arg-H$^{\gamma}$, 8 × Leu-H$^{\beta}$, 4 × Leu-H$^{\gamma}$), 3.05−3.21 (m, 8H, 8 × Arg-H$^{\beta}$), 5.53−6.35 (m, 22H, 17 × H1′ sugar ring protons, 5 × H5 of dC), 7.27−8.36 (m, 23H, 23 × Ar−H from dG (×4), dA (×12), dC (×5), and dT (×2). The H3′/H4′/H5′/H5″ sugar ring proton regions (3.5−5.0 ppm) were not analyzed due to suppression of residual water signal at 4.8 ppm. $^{31}P\{^1H\}$ NMR (D_2O, 160 MHz): δ −1.54 to −0.91 (16P, $\underline{P}O_4$), 5.84 (1P, N-$\underline{P}O_3$). No sample reference was used for ^{31}P NMR analysis. It was carried out to observe the relative shift of the ^{31}P−N resonance.

*P2-A-COOH (**10**).* Fractions at 29 min were collected, combined, and lyophilized. The excess salt was removed by dissolving the material in H_2O (100 μL) and precipitating in 4% $LiClO_4$ in acetone (w/v) (1.8 mL) overnight. The product was collected by centrifugation (13 400 rpm, 4 min), air-dried, and then freeze−dried to give a white powder (8.4 nmol, 70%). MALDI-MS: m/z = 2952 $[M+H+K]^{2+}$, 5902 $[M+K]^+$ (MW = 5863 calcd. for $[C_{191}H_{259}N_{80}O_{104}P_{17}]$). ^1H NMR (D_2O with TSP (0.01 μM), 400 MHz): δ 0.65−0.85 (m, 12H, Leu-H$^{\delta}$), 1.29−2.85 (m, 54H, 17 × H2′ and 17 × H2″ sugar ring protons, 2 × CH_3 of 2 × dT, 4 × Arg-H$^{\delta}$, 4 × Arg-H$^{\gamma}$, 4 × Leu-H$^{\beta}$, 2 × Leu-H$^{\gamma}$), 3.00−3.10 (m, 4H, 4 × Arg-H$^{\beta}$), 5.42−6.23 (m, 22H, 17 × H1′ sugar ring protons, 5 × H5 of dC), 7.20−8.27 (m, 23H, 23 × Ar−H from dG (×4), dA (×12), dC (×5), and dT (×2). The H3′/H4′/H5′/H5″ sugar ring proton regions (3.5−5.0 ppm) were not analyzed due to suppression of residual water signal at 4.8 ppm. $^{31}P\{^1H\}$ NMR (D_2O, 160 MHz): δ −1.43 to −0.98 (16P, $\underline{P}O_4$), 6.04 (1P, N-$\underline{P}O_3$). No sample reference was used for ^{31}P NMR analysis. It was carried out to observe the relative shift of the ^{31}P−N resonance.

Preparation of Linearized Plasmid p67YF0. The reaction mixture (1 mL) contained 10 mM Tris-HCl pH 7.6, 10 mM $MgCl_2$, 50 mM NaCl, 1 mM DTT, 100 μg p67YF90,[37] and 750 units of Bst2UI restriction endonuclease. Restriction was carried out for 1.5 h at 60 °C. Reaction was quenched by phenol:chloroform (1:1, v/v) extraction followed by ethanol precipitation. After centrifugation, linearized plasmid p67YF0 was rinsed twice with 70% ethanol and dissolved in water. Linearized plasmid p67YF0 was stored in water at −20 °C until use.

Preparation of Linearized Plasmid pHIV-2. The reaction mixture (1 mL) contained 33 mM Tris-acetate pH 7.9, 10 mM $MgAc_2$, 66 mM KAc, 1 mM DTT, 100 μg pHIV-2, and 100 units of FokI restriction endonuclease. Restriction was carried out for 1 h at 37 °C. Reaction was quenched by phenol:chloroform (1:1, v/v) extraction followed by ethanol precipitation. After centrifugation, linearized plasmid pHIV-2 was rinsed twice with 70% ethanol and dissolved in water. Linearized plasmid pHIV-2 was stored in water at −20 °C until use.

Preparation of in Vitro Transcript of Yeast tRNA^{Phe} and HIV-RNA. tRNA^{Phe} and HIV-RNA were prepared by in vitro transcription with T7 RNA polymerase using Bst2U1-linearized plasmid p67YF0 and Fok1-linearized plasmid pHIV-2, respectively. The reaction mixture (100 μL) contained 40 mM Tris-HCl pH 8.0, 6 mM $MgCl_2$, 2 mM spermidine, 10 mM NaCl, 10 mM DTT, 1 mM each of NTP, 10 μg of DNA, and 75 units of T7 RNA polymerase. Transcription was carried out for 2 h at 37 °C. Reaction was quenched by phenol:chloroform (1:1 v/v) extraction followed by ethanol precipitation. After centrifugation, RNA precipitate was rinsed twice with 70% ethanol and dissolved in loading buffer (8 M urea, 20 mM EDTA, 0.025% bromophenol blue, 0.025% xylene cyanol). RNA transcripts were isolated using electrophoresis in 6% PAA/8 M urea gel and TBE (100 mM Tris−borate pH 8.3, 20 mM EDTA) as running buffer. RNA transcripts were cut out of the gel and eluted using 3 × 300 μL elution buffer (0.3 M NaAc pH 5.0, 10% v/v phenol pH 6.0), precipitated with ethanol, and stored until use.

DOI: 10.1021/acs.bioconjchem.5b00193
Bioconjugate Chem. 2015, 26, 1129−1143

3′-End Labeling of RNA Transcript with Fluorescein Isothiocyanate (FITC). The reaction mixture (100 μL) containing 50 μg $tRNA^{Phe}$ or HIV-RNA, 20 mM ethylenediamine-HCl pH 6.8, 1 mM sodium periodate, and 10% EtOH was incubated at 0 °C for 10 min in the dark. After incubation 11 mL of 50% glycerol was added and the mixture was incubated for 30 min at 37 °C. After incubation 38 mL of 0.3 M sodium cyanoborohydride was added and the mixture was incubated for 30 min at room temperature. The reaction was quenched by ethanol precipitation. $tRNA^{Phe}$ or HIV-RNA was collected by centrifugation and dissolved in 20 μL water and then 10 μL of triethylamine, 60 μL of DMSO, and 10 μL of 0.3 M FITC in DMSO were added. The mixture was shaken for 1 h at room temperature and the reaction was quenched by ethanol precipitation. Labeled RNA was collected by centrifugation and dissolved in loading buffer (8 M urea, 20 mM EDTA, 0.025% bromophenol blue, 0.025% xylene cyanol).). Labeled RNA was isolated using denaturating electrophoresis as described above. Labeled RNA was cut out of the gel and eluted using 3 × 300 μL of elution buffer (0.3 M NaAc pH 5.0, 10% phenol pH 6.0) and precipitated with ethanol. Labeled RNA was stored until use at −20 °C in 70% ethanol.

3′-FITC $tRNA^{Phe}$ Binding with Peptidyl−Oligonucleotide Conjugates. The reaction mixture (5 μL) contained 0.5 μM 3′-FITC-$tRNA^{Phe}$, one of the POCs at concentrations ranging from 0.5 to 20 μM, 50 mM Tris−HCl pH 7.0, 0.2 M KCl, 1 mM EDTA. The mixtures were incubated at 37 °C for 30 min. Then 5 μL of loading buffer (20% ficoll, 0.025% bromophenol blue, 0.025% xylene cyanol) was added. 3′-FITC-$tRNA^{Phe}$ and 3′-FITC-$tRNA^{Phe}$/POC complexes were resolved in 10% polyacrylamide gel using TBE (100 mM Tris−borate pH 8.3, 20 mM EDTA) as running buffer at 4 °C. The gel was analyzed using Molecular Imager FX (Bio-Rad). To obtain quantitative data, gel images were processed with *GelPro Analyzer* and graphs were built using *OriginPro 8*.

Cleavage of 3′-FITC Labeled $tRNA^{Phe}$ or 3′-FITC Labeled HIV-RNA with Peptidyl−Oligonucleotide Conjugates. The reaction mixture (5 μL) contained 3′-FITC-$tRNA^{Phe}$ or 3′-FITC-HIV-RNA at concentration 1 μM, one of the POCs at concentrations ranging from 1 to 40 μM (20 μM in the case of kinetic experiments), 50 mM Tris−HCl pH 7.0, 0.2 M KCl, and 1 mM EDTA. In some experiments, the reaction mixtures contained additionally 5 mM $MgCl_2$.or oligonucleotide **A** (50 μM). The mixtures were incubated at 37 °C (for various times) and quenched by RNA precipitation with 2% lithium perchlorate in acetone (75 μL). RNA pellet was collected by centrifugation and dissolved in loading buffer (8 M urea, 0.025% bromophenol blue, 0.025% xylene cyanol). RNA cleavage products were resolved in 12% polyacrylamide/8 M urea gel using TBE as running buffer. To identify cleavage sites, an imidazole ladder[38] and a RNase T1-ladder[39] produced by partial $tRNA^{Phe}$ cleavage with 2 M imidazole buffer (pH 7.0) and RNase T1, respectively, were run in parallel. The gel was analyzed using *Molecular Imager FX* (Bio-Rad). To obtain quantitative data, gels images were processed with *GelPro Analyzer* and graphs were built using *OriginPro 8*.

■ ASSOCIATED CONTENT

Ⓢ Supporting Information

POC MALDI-ToF mass spectra; and additional gel-electrophoresis data is avaliable. The Supporting Information is available free of charge on the ACS Publications website at DOI: 10.1021/acs.bioconjchem.5b00193.

■ AUTHOR INFORMATION

Corresponding Author

*E-mail: aled.williams@manchester.ac.uk.

Author Contributions

#Aled Williams and Yaroslav Staroseletz contributed equally to the work.

Notes

The authors declare no competing financial interest.

■ ACKNOWLEDGMENTS

This research has been supported by the EPSRC (Grant No. EP/G017905/1), Collaborative Research Framework Agreement with SOLVAY (Work Program 2), and by the Russian Science Foundation (Grant No. 14-44-00068). We are grateful to the National Mass Spectrometry Centre (Swansea, U.K.) for carrying out the peptide mass spectrometery analysis and Catherine Watson (Manchester Pharmacy School) for the $tRNA^{Phe}$ structrure analysis using YASARA NOVA.[55]

■ ABBREVIATIONS

ASO, antisense oligonucleotide; POC, peptidyl−oligonucleotide conjugate; FITC, fluorescein isothiocyanate; DEPC, diethylpyrocarbonate; TSP, trimethylsilyl propanoic acid

■ REFERENCES

(1) Manoharan, M. (2002) Oligonucleotide conjugates as potential antisense drugs with improved uptake, biodistribution, targeted delivery, and mechanism of action. *Antisense Nucleic Acid Drug Dev. 12*, 103−128.

(2) HÄNer, R., and Hall, J. (1997) The sequence-specific cleavage of RNA by artificial chemical ribonucleases. *Antisense Nucleic Acid Drug Dev. 7*, 423−430.

(3) Kole, R., Krainer, A. R., and Altman, S. (2012) RNA therapeutics: beyond RNA interference and antisense oligonucleotides. *Nat. Rev. Drug Discovery 11*, 125−140.

(4) Garzon, R., Marcucci, G., and Croce, C. M. (2010) Targeting microRNAs in cancer: rationale, strategies and challenges. *Nat. Rev. Drug Discovery 9*, 775−789.

(5) Zhao, X., Pan, F., Holt, C. M., Lewis, A. L., and Lu, J. R. (2009) Controlled delivery of antisense oligonucleotides: a brief review of current strategies. *Expert Opin. Drug Delivery 6*, 673−686.

(6) Khan, A. A., Betel, D., Miller, M. L., Sander, C., Leslie, C. S., and Marks, D. S. (2009) Transfection of small RNAs globally perturbs gene regulation by endogenous microRNAs. *Nat. Biotechnol. 27*, 549−555.

(7) Mironova, N. L., Pyshnyi, D. V., Ivanova, E. M., Zarytova, V. F., Zenkova, M. A., Gross, H. J., and Vlassov, V. V. (2002) Sequence-specific RNA cleavage by oligonucleotide-peptide conjugates. *Russ. Chem. Bull. 51*, 1177−1186.

(8) Mironova, N. L., Pyshnyi, D. V., Shtadler, D. V., Fedorova, A. A., Vlassov, V. V., and Zenkova, M. A. (2007) RNase T1 mimicking artificial ribonuclease. *Nucleic Acids Res. 35*, 2356−2367.

(9) Mironova, N. L., Pyshnyi, D. V., Ivanova, E. M., Zenkova, M. A., Gross, H. J., and Vlassov, V. V. (2004) Covalently attached oligodeoxyribonucleotides induce RNase activity of a short peptide and modulate its base specificity. *Nucleic Acids Res. 32*, 1928−1936.

(10) Niittymaki, T., and Lonnberg, H. (2006) Artificial ribonucleases. *Org. Biomol. Chem. 4*, 15−25.

(11) Lonnberg, H. (2011) Cleavage of RNA phosphodiester bonds by small molecular entities: a mechanistic insight. *Org. Biomol. Chem. 9*, 1687−1703.

(12) Morrow, J. R. (2008) Speed limits for artificial ribonucleases. *Comment Inorg. Chem. 29*, 169−188.

DOI: 10.1021/acs.bioconjchem.5b00193
Bioconjugate Chem. 2015, 26, 1129−1143

(13) Bashkin, J. K., Frolova, E. I., and Sampath, U. (1994) Sequence-specific cleavage of HIV mRNA by a ribozyme mimic. *J. Am. Chem. Soc. 116*, 5981−5982.
(14) Trawick, B. N., Osiek, T. A., and Bashkin, J. K. (2001) Enhancing sequence-specific cleavage of RNA within a duplex region: incorporation of 1,3-propanediol linkers into oligonucleotide conjugates of serinol−terpyridine. *Bioconjugate Chem. 12*, 900−905.
(15) Putnam, W. C., Daniher, A. T., Trawick, B. N., and Bashkin, J. K. (2001) Efficient new ribozyme mimics: direct mapping of molecular design principles from small molecules to macromolecular, biomimetic catalysts. *Nucleic Acids Res. 29*, 2199−2204.
(16) Magda, D., Crofts, S., Lin, A., Miles, D., Wright, M., and Sessler, J. L. (1997) Synthesis and kinetic properties of ribozyme analogues prepared using phosphoramidite derivatives of dysprosium(III) texaphyrin. *J. Am. Chem. Soc. 119*, 2293−2294.
(17) Hall, J., Hüsken, D., and Häner, R. (1996) Towards artificial ribonucleases: the sequence-specific cleavage of RNA in a duplex. *Nucleic Acids Res. 24*, 3522−3526.
(18) Matsuda, S., Ishikubo, A., Kuzuya, A., Yashiro, M., and Komiyama, M. (1998) Conjugates of a dinuclear zinc(II) complex and DNA oligomers as novel sequence-selective artificial ribonucleases. *Angew. Chem., Int. Ed. 37*, 3284−3286.
(19) Putnam, W. C., and Bashkin, J. K. (2000) synthesis of artificial ribonucleases with benign metal catalysts. *Chem. Commun.*, 767−768.
(20) Beloglazova, N. G., Fabani, M. M., Polushin, N. N., Sil, #39, nikov, V. V., Vlassov, V. V., Bichenkova, E. V., and Zenkova, M. A. (2011) Site-selective artificial ribonucleases: oligonucleotide conjugates containing multiple imidazole residues in the catalytic domain. *J. Nucleic Acids 2011*, 17.
(21) Nakano, S.-i., Uotani, Y., Uenishi, K., Fujii, M., and Sugimoto, N. (2004) Site-selective RNA cleavage by DNA bearing a base pair-mimic nucleoside. *J. Am. Chem. Soc. 127*, 518−519.
(22) Kuzuya, A., Mizoguchi, R., and Komiyama, M. (2001) Site-selective artificial ribonuclease using pinpoint RNA activation. *Nucl. Acid S. 1*, 131−132.
(23) Niittymäki, T., Kaukinen, U., Virta, P., Mikkola, S., and Lönnberg, H. (2003) Preparation of azacrown-functionalized 2′-O-methyl oligoribonucleotides, potential artificial RNases. *Bioconjugate Chem. 15*, 174−184.
(24) Niittymäki, T., Virta, P., Ketomäki, K., and Lönnberg, H. (2007) Di(azacrown) conjugates of 2′-O-methyl oligoribonucleotides as sequence-selective artificial ribonucleases. *Bioconjugate Chem. 18*, 1583−1592.
(25) Niittymäki, T., and Lönnberg, H. (2004) Sequence-selective cleavage of oligoribonucleotides by 3d transition metal complexes of 1,5,9-triazacyclododecane-functionalized 2′-O-methyl oligoribonucleotides. *Bioconjugate Chem. 15*, 1275−1280.
(26) Magda, D., Miller, R. A., Sessler, J. L., and Iverson, B. L. (1994) Site-specific hydrolysis of RNA by europium(III) texaphyrin conjugated to a synthetic oligodeoxyribonucleotide. *J. Am. Chem. Soc. 116*, 7439−7440.
(27) Morrow, J. R., Buttrey, L. A., Shelton, V. M., and Berback, K. A. (1992) Efficient catalytic cleavage of RNA by lanthanide(III) macrocyclic complexes: toward synthetic nucleases for in vivo applications. *J. Am. Chem. Soc. 114*, 1903−1905.
(28) Canaple, L., Hüsken, D., Hall, J., and Häner, R. (2002) Artificial ribonucleases: efficient and specific in vitro cleavage of human c-raf-1 RNA. *Bioconjugate Chem. 13*, 945−951.
(29) Petyuk, V. A., Zenkova, M. A., Giege, R., and Vlassov, V. V. (1999) Hybridization of antisense oligonucleotides with the 3′ part of tRNAPhe. *FEBS Lett. 444*, 217−221.
(30) Kumazawa, Y., Yokogawa, T., Tsurui, H., Miura, K.-i., and Watanabe, K. (1992) Effect of the higher-order structure of tRNAs on the stability of hybrids with oligodeoxyribonucleotides: separation of tRNA by an efficient solution hybridization. *Nucleic Acids Res. 20*, 2223−2232.
(31) Frankel, A. D. (1992) Peptide models of the tat—Tar protein-RNA interaction. *Protein Sci. 1*, 1539−1542.
(32) Puglisi, J., Tan, R., Calnan, B., Frankel, A., and Williamson (1992) Conformation of the TAR RNA-arginine complex by NMR spectroscopy. *Science 257*, 76−80.
(33) Sermon, B. A., Lowe, P. N., Strom, M., and Eccleston, J. F. (1998) The importance of two conserved arginine residues for catalysis by the Ras GTPase-activating protein, neurofibromin. *J. Biol. Chem. 273*, 9480−9485.
(34) Pace, C. N., Heinemann, U., Hahn, U., and Saenger, W. (1991) Ribonuclease T1: structure, function, and stability. *Angew. Chem., Int. Ed. 30*, 343−360.
(35) Ariga, K., and Anslyn, E. V. (1992) Manipulating the stoichiometry and strength of phosphodiester binding to a bisguanidine cleft in DMSO/water solutions. *J. Org. Chem. 57*, 417−419.
(36) Schug, K. A., and Lindner, W. (2005) Noncovalent binding between guanidinium and anionic groups: focus on biological- and synthetic-based arginine/guanidinium interactions with phosph[on]ate and sulf[on]ate residues. *Chem. Rev. 105*, 67−114.
(37) Yan, B. X., and Sun, Y. Q. (1997) Glycine residues provide flexibility for enzyme active sites. *J. Biol. Chem. 272*, 3190−3194.
(38) Bartlett, G. J., Porter, C. T., Borkakoti, N., and Thornton, J. M. (2002) Analysis of catalytic residues in enzyme active sites. *J. Mol. Biol. 324*, 105−121.
(39) Okoniewska, M., Tanaka, T., and Yada, R. Y. (2000) The pepsin residue glycine-76 contributes to active-site loop flexibility and participates in catalysis. *Biochem. J. 349*, 169−177.
(40) Tiwari, M. K., Singh, R. K., Singh, R., Jeya, M., Zhao, H., and Lee, J.-K. (2012) Role of conserved glycine in zinc-dependent medium chain dehydrogenase/reductase superfamily. *J. Biol. Chem. 287*, 19429−19439.
(41) Zarytova, V. F., Ivanova, E. M., Yarmolyuk, S. N., and Alekseeva, I. V. (1988) Synthesis of arginine-containing oligonucleotide-5′-N-peptides. *Biopolimery i Kletka 4*, 220−222.
(42) Silnikov, V., Zuber, G., Behr, J. P., Giege, R., and Vlassov, V. (1996) Design of ribonuclease mimics for sequence specific cleavage of RNA. *Phosphorus Sulfur Silicon 277−280*, 109−110.
(43) Beloglazova, N. G., Sil'nikov, V. N., Zenkova, M. A., and Vlassov, V.V. . (2000) Sequence-specific cleavage of yeast tRNAPhe with oligonucleotides conjugated to a diimidazole construct. *Antisense Nucleic Acid Drug Dev.*, 39−42.
(44) Beloglazova, N. G., Sil'nikov, V. N., Zenkova, M. A., and Vlassov, V. V. (2000) Cleavage of yeast tRNAPhe with complementary oligonucleotide conjugated to a small ribonuclease mimic. *FEBS Lett. 481*, 277−280.
(45) Beloglazova, N. G., Fabani, M. M., Zenkova, M. A., Bichenkova, E. V., Polushin, N. N., Sil'nikov, V. V., Douglas, K. T., and Vlassov, V. V. (2004) Sequence-specific artificial ribonucleases. I. Bis-imidazole-containing oligonucleotide conjugates prepared using precursor-based strategy. *Nucleic Acids Res. 32*, 3887−3897.
(46) Serikov, R., Petyuk, V., Vorobijev, Y., Koval, V., Fedorova, O., Vlassov, V., and Zenkova, M. (2011) Mechanism of antisense oligonucleotide interaction with natural RNAs. *J. Biomol. Struct. Dyn. 29*, 27−50.
(47) Vlassov, V. V., Zuber, G., Felden, B., Behr, J.-P., and Giegè, R. (1995) Cleavage of tRNA with imidazole and spermine imidazole constructs: a new approach for probing RNA structure. *Nucleic Acids Res. 23*, 3161−3167.
(48) Serikov, R. N., P, V. N., Vlassov, V. V., and Zenkova, M. A. (2002) Hybridization of antisense oligonucleotides with yeast tRNAPhe: factors determining the efficiency of interaction. *Russ. Chem. Bull. Int. Ed. 51*, 1156−1165.
(49) Kuznetsova, I. L., Zenkova, M. A., Gross, H. J., and Vlassov, V. V. (2005) Enhanced RNA cleavage within bulge-loops by an artificial ribonuclease. *Nucleic Acids Res. 33*, 1201−1212.
(50) Jin, Y., and Cowan, J. A. (2006) Targeted cleavage of HIV Rev response element RNA by metallopeptide complexes. *J. Am. Chem. Soc. 128*, 410−411.
(51) Romby, P., Moras, D., Bergdoll, M., Dumas, P., Vlassov, V. V., Westhof, E., Ebel, J. P., and Giegé, R. (1985) Yeast tRNAAsp tertiary

DOI: 10.1021/acs.bioconjchem.5b00193
Bioconjugate Chem. 2015, 26, 1129−1143

structure in solution and areas of interaction of the tRNA with aspartyl-tRNA synthetase: A comparative study of the yeast phenylalanine system by phosphate alkylation experiments with ethylnitrosourea. *J. Mol. Biol. 184*, 455−471.
(52) Giegé, R., Felden, B., Zenkova, M. A., Sil'nikov, V. N., and Vlassov, V. V. (2000) [11] Cleavage of RNA with synthetic ribonuclease mimics, in *Methods in Enzymology*, pp 147−165, Academic Press.
(53) Hingerty, B., Brown, R. S., and Jack, A. (1978) Further refinement of the structure of yeast tRNAPhe. *J. Mol. Biol. 124*, 523−34.
(54) Shi, H., and Moore, P. B. (2000) The crystal structure of yeast phenylalanine tRNA at 1.93 A resolution: a classic structure revisited. *RNA 6*, 1091−105.
(55) Krieger, E., Koraimann, G., and Vriend, G. (2002) Increasing the precision of comparative models with YASARA NOVA—a self-parameterizing force field. *Proteins: Struct., Funct., Bioinf. 47*, 393−402.
(56) Corona-Martinez, D. O., Taran, O., and Yatsimirsky, A. K. (2010) Mechanism of general acid-base catalysis in transesterification of an RNA model phosphodiester studied with strongly basic catalysts. *Org. Biomol. Chem. 8*, 873−880.
(57) Oost, T., and Kalesse, M. (1997) Synthesis of RNAse active site model systems using a steroid template. *Tetrahedron 53*, 8421−8438.
(58) Kubiak, R. J., Yue, X., Hondal, R. J., Mihai, C., Tsai, M.-D., and Bruzik, K. S. (2001) Involvement of the Arg−Asp−His catalytic triad in enzymatic cleavage of the phosphodiester bond†. *Biochemistry 40*, 5422−5432.
(59) Arni, R. K., Watanabe, L., Ward, R. J., Kreitman, R. J., Kumar, K., and Walz, F. G. (1999) Three-dimensional structure of ribonuclease T1 complexed with an isosteric phosphonate substrate analogue of GpU: alternate substrate binding modes and catalysis. *Biochemistry 38*, 2452−2461.
(60) Mironova, N. L., Pyshnyi, D. V., Stadler, D. V., Prokudin, I. V., Boutorine, Y. I., Ivanova, E. M., Zenkova, M. A., Gross, H. J., and Vlassov, V. V. (2006) G-specific RNA-cleaving conjugates of short peptides and oligodeoxyribonucleotides. *J. Biomol. Struct. Dyn. 23*, 591−602.
(61) Crooke, S. T., and Bennett, C. F. (1996) Progress in antisense oligonucleotide therapeutics. *Annu. Rev. Pharmacol. 36*, 107−129.
(62) Stein, C. A., and Cheng, Y. C. (1993) Antisense oligonucleotides as therapeutic agents-is the bullet really magical? *Science 261*, 1004−1012.
(63) Andrea, D. B. (1998) A good antisense molecule is hard to find. *Trends Biochem. Sci. 23*, 45−50.
(64) Riguet, E., Tripathi, S., Chaubey, B., Désiré, J., Pandey, V. N., and Décout, J.-L. (2004) A peptide nucleic acid−neamine conjugate that targets and cleaves HIV-1 TAR RNA inhibits viral replication†. *J. Med. Chem. 47*, 4806−4809.

DOI: 10.1021/acs.bioconjchem.5b00193
Bioconjugate Chem. 2015, 26, 1129−1143